Studies on Electrochemical Responses of Molecular Compounds in Homogeneous Solution under Photoirradiation

FUKATSU ARISA

Doctor of Philosophy

Department of Structural Molecular Science
School of Physical Sciences
SOKENDAI (The Graduate University for Advanced Studies)

Studies on Electrochemical Responses of Molecular Compounds in Homogeneous Solution under Photoirradiation

光照射下における溶存分子化合物の電気化学応答に関する研究

Arisa Fukatsu

March 2018

Department of Structural Molecular Science
School of Physical Sciences
SOKENDAI (The Graduate University for Advanced Studies)

Contents

General Introduction

1. Electrochemical analyses of molecular compounds under photoirradiation

Photochemical reactions of organic compounds [1-3] and transition metal complexes [4-6] have been widely studied not only because of their fundamental importance in chemistry but also because they serve as model reactions of biophysical phenomena such as photosynthesis [7,8] and phototransduction [9,10]. In addition, a detailed understanding of the mechanisms of such photochemical reactions would provide deeper insight into future technological applications including artificial photosynthesis [11-13] and optogenetics [14,15]. Because a photochemical reaction consists of an initial photoexcitation process and subsequent multistep exothermic processes, analyzing the intermediates generated during the reactions is essential to understanding the mechanisms of photochemical reactions of molecular compounds.

Electrochemical measurements, *e.g.*, cyclic voltammetry, are a well-established analytical means to evaluate the HOMOs and LUMOs of molecular substrates by observation of the electrical current attributed to electron transfer between the substrates and the electrode. Because the electronic structures of the substrates are changed upon photoexcitation, *in-situ* observation of the electrochemical response under photoirradiation can be a powerful technique to investigate the photochemical reaction mechanisms. However, electrochemical analyses under photoirradiation for molecular substrates in homogeneous solution are not widely performed at present, although those for heterogeneous systems have been extensively used in the fields of solar cells and semiconductor photocatalysts. [16-18]

From a historical point of view, electrochemical analyses under photoirradiation for molecular substrates in homogeneous solution are not an unexplored research topic. The first pioneering work on such measurements, photopolarography, was reported in 1960, by using a dropping mercury electrode as the working electrode, as described in Section 2.1. [19-42]. In the 1970s, the special rotating electrode, composed of an inert-metal ring electrode and an optically

transparent disk, was developed and used to detect the electrochemical responses of photochemically generated intermediates (Section 2.2) [19,43-51]. In the 1980s, by adopting the modulation principle in photoelectrochemical measurements, a technique called photomodulation voltammetry was developed to detect the redox current of short-lived transient species (Section 2.3) [52-62]. These photoelectrochemical techniques were separately developed by different research groups in different periods by using different experimental setups (Table 1), although they were developed with a common objective, to some extent.

Table 1. List of photoelectrochemical systems used to perform electrochemical measurements of molecular substrates in homogeneous solution under photoirradiation.

Section	Photoelectrochemical System	Period	Working Electrode	Light	Target[a)]
2.1.	Photopolarography	1960s-	dropping mercury electrode	continuous / pulse	A
2.2.	Rotating photoelectrode technique	1970s-	rotating electrode	continuous	A
2.3.	Photomodulation voltammetry	1980s-	planar electrode	pulse	B, C

[a)] A: detection of intermediates of photochemical reactions, B: analysis of redox potentials of transient species, C: analysis of lifetimes of transient species.

2. Overview of photoelectrochemical systems for molecular substrates

2.1. Photopolarography

The research on electrochemical measurements of molecular substrates in solution under photoirradiation began with the detection of the photocurrent attributed to photochemically generated species by using a mercury electrode. [20-42] This system, photopolarography, was first reported by Berg *et al.* in 1960. In a typical setup in this system, an electrochemical cell composed of a three-electrode configuration in conjunction with a potentiostat is used (Fig. 1). Photochemical reaction is initiated by irradiating the solution with either a continuous or a flashing light close to a dropping mercury electrode used as the working electrode.

In pioneering work by Berg and coworkers, [23] the photodimerization reaction of benzophenone (Eqs. (1)-(4) in Scheme 1) was analyzed. A solution of benzophenone in an isopropanol-water mixed solvent with sodium hydroxide was photoirradiated by a high-pressure mercury lamp or argon lamp, and chronoamperometry was performed on the solution by using photopolarography. As a result, current was observed, which was attributed to the oxidative reactions of a benzophenone ketyl radical and a benzopinacol anion (Eqs. (5) and (6) in Scheme 1). The rate constant (k) of the dimerization reaction of the benzophenone ketyl radical (Eq. (4) in Scheme 1) was evaluated from the current-time curve. The authors also investigated the photochemical reaction kinetics of hydroquinones [20-22,26] and other organic compounds [24-32].

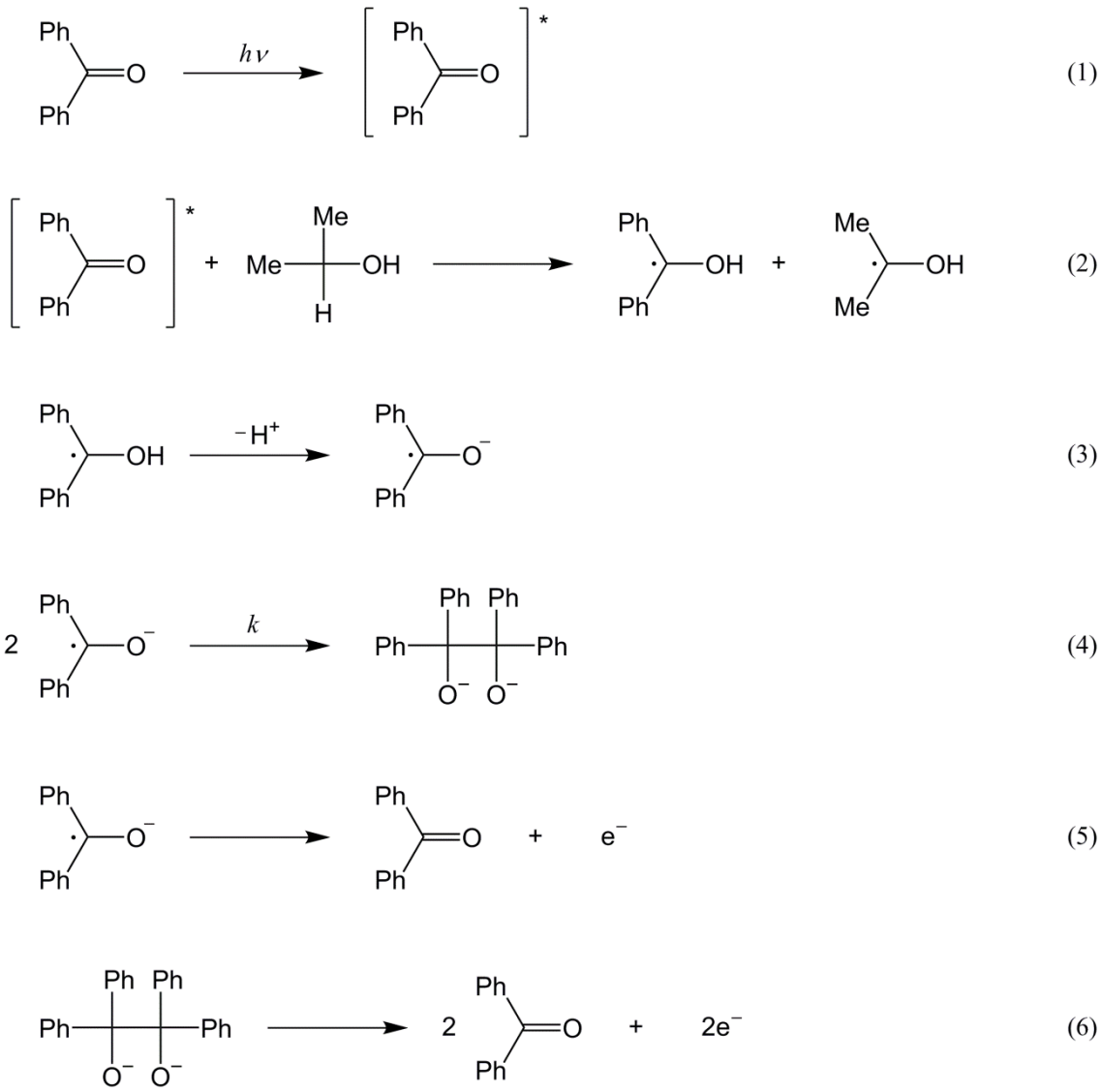

Scheme 1. Eqs. (1)-(4): Reaction sequence of the photolysis of benzophenone in a basic isopropanol-water solvent. Eqs. (5)-(6): Electrochemical reaction of the electroactive species formed during photolysis.

This system was also applied to the photochemical reaction of a metal complex by Imai and coworker. [33] In this study, the photochemical reduction of trisoxalatoferrate(III) ($\mathbf{[Fe(ox)_3]^{3-}}$) in the presence of potassium oxalate was analyzed. In this reaction, the excited state of $\mathbf{[Fe^{III}(ox)_3]^{3-}}$, *i.e.*, $\mathbf{[Fe^{III}(ox)_3]^{3-*}}$, is reduced by an oxalate anion, thus yielding the reduced species $\mathbf{[Fe^{II}(ox)_3]^{4-}}$ (Eqs. (7) and (8) in Scheme 2) Chronoamperometry of $\mathbf{[Fe(ox)_3]^{3-}}$ in aqueous solution with potassium oxalate under continuous photoirradiation detected the anodic current corresponding to the oxidation of $\mathbf{[Fe^{II}(ox)_3]^{4-}}$ (Eq. (9) in Scheme 2).

$$[Fe^{III}(ox)_3]^{3-} \xrightarrow{h\nu} [Fe^{III}(ox)_3]^{3-*} \quad (7)$$

$$[Fe^{III}(ox)_3]^{3-*} + 1/2C_2O_4^{2-} \longrightarrow [Fe^{II}(ox)_3]^{4-} + CO_2 \quad (8)$$

$$[Fe^{II}(ox)_3]^{4-} \longrightarrow [Fe^{III}(ox)_3]^{3-} + e^- \quad (9)$$

Scheme 2. Eqs. (7), (8): Reaction sequence of the photolysis of $\mathbf{[Fe(ox)_3]^{3-}}$ with an oxalate anion. Eq. (9): Electrochemical reaction of the electroactive species generated by the photolysis.

As described above, analyzing the current-time profiles obtained by photopolarography enabled the kinetic study of several types of photochemical reactions. However, this approach is inaccurate because of the general difficulty in developing a theory for kinetic currents at the dropping electrode. Moreover, the second-order kinetic processes due to the expanding mercury drop create additional complications in analyzing the obtained current responses. To overcome the problems of this initially developed photopolarography system, a system using a hanging mercury drop electrode, which steadily releases drops of mercury during an experiment, was developed. [35-42] Because this system can provide the steady surface of the electrode, the complication in current response caused by the growing surface area of a dropping electrode has been overcome. As a result, the quantitative accuracy of the kinetic analysis was improved.

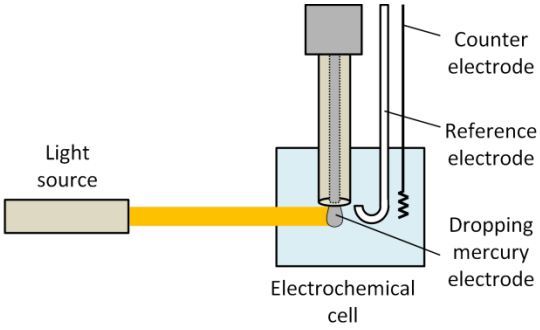

Fig. 1. A typical photopolarography setup.

2.2. Rotating photoelectrode technique

The second system for electrochemical measurements under photoirradiation was developed by Johnson and coworkers in 1972. [43] They used a modified rotating electrode, the rotating photoelectrode (RPE) (Fig. 2), to study the photochemical reactions in solution. The RPE is composed of an inert-metal ring electrode and an optically transparent disk. A collimated beam of light is passed through the transparent disk of the RPE. The products of photochemical reactions occurring in the vicinity of the disk are transported by convective-diffusional processes to the surface of the ring electrode, and the electrochemical responses of the products are detected.

In this system, the change in the rotating speed of the RPE provides information that can be used to characterize the electrochemically detected species. A general reaction sequence of photolysis is shown in Scheme 3. In this reaction, **A** is initially converted to **B** by photoexcitation, and the subsequent chemical reaction yields the product, **C**. If **B** is electrochemically active and **C** is not, the ring current should increase as the rotational velocity of the photoelectrode increases. Conversely, if **C** is electrochemically active and **B** is not, the ring current will decrease as the rotational velocity increases.

$$\mathrm{A} \xrightarrow{h\nu} \mathrm{B} \qquad (10)$$

$$\mathrm{B} \longrightarrow \mathrm{C} \qquad (11)$$

Scheme 3. Eq. (10): Photoexcitation process. Eq. (11) Subsequent chemical reaction.

In the first report by Johnson and coworkers, [43] photolysis of benzophenone and $\mathbf{[Fe(ox)_3]^{3-}}$ was investigated using the RPE system. Controlled potential electrolysis (CPE) of benzophenone was performed in an ethanol-water solution with sodium hydroxide at $E = -0.8$ V *vs.* SCE under photoirradiation, and current attributed to the oxidation of the benzophenone ketyl radical (Eq. (5) in Scheme 1) was observed. Notably, only the ketyl radical is an electrochemically active species under the applied conditions. In the photochemical reaction of benzophenone, a ketyl radical of benzophenone is generated by the chemical reactions (Eqs. (2) and (3) in Scheme 1) that

proceed after the photoexcitation (Eq. (1)), and the further reaction of a ketyl radical yields a benzopinacol anion (Eq. (4)). In other words, a ketyl radical can be regarded as a reactive intermediate in this photochemical reaction. In fact, the plot of the ring current as a function of the angular velocity of electrode rotation, ω, has a positive slope, thus suggesting that the reactive intermediate is electroactive.

In the case of $\mathbf{[Fe^{III}(ox)_3]^{3-}}$, CPE was performed using RPE in an aqueous solution with sulfuric acid at E = 0.55 V, and current attributed to the oxidation of $\mathbf{[Fe^{II}(ox)_3]^{4-}}$ was observed. In the photochemical reaction of $\mathbf{[Fe^{III}(ox)_3]^{3-}}$, flash photolysis results in the production of a metastable intermediate, and the further reaction of the intermediate yields $\mathbf{[Fe^{II}(ox)_3]^{4-}}$ and carbon dioxide as the final products. In CPE experiment, the current attributed to the oxidation of $\mathbf{[Fe^{II}(ox)_3]^{4-}}$ decreased as ω was increased, as expected if $\mathbf{[Fe^{II}(ox)_3]^{4-}}$ is produced by the chemical reaction of a metastable photoproduct.

The authors also described a digital simulation of the processes occurring at the RPE that affect the production, consumption, and mass transport of the photoproducts. [44] The current response obtained by the RPE system was analyzed by digital simulation to investigate the kinetics of the photodimerization of benzophenone. The obtained rate constant was in fairly good agreement with the literature values obtained by other methods.

Mann and coworkers applied the RPE system to voltammetric study. [46] In their study, photolysis of $\mathbf{CpFe(\eta^6\text{-}p\text{-}xyl)^+}$ ($Cp^- = \eta^5\text{-}C_5H_5^-$; xyl = xylene) (Eqs. (12) and (13) in Scheme 4) was analyzed. Linear sweep voltammetry of $\mathbf{CpFe(\eta^6\text{-}p\text{-}xyl)^+}$ in an acetonitrile solution with tetra-*n*-butylammonium hexafluorophosphate was performed under photoirradiation. Photocurrent due to the oxidation of $\mathbf{CpFe(CH_3CN)_3^+}$ intermediate (Eq. (14) in Scheme 4) was detected at ω = 267 rad/s.

$$CpFe(\eta^6\text{-}p\text{-xyl})^+ \xrightarrow{h\nu} CpFe(\eta^6\text{-}p\text{-xyl})^{+*} \quad (12)$$

$$CpFe(\eta^6\text{-}p\text{-xyl})^{+*} + 3MeCN \longrightarrow CpFe(MeCN)_3^+ + p\text{-xyl} \quad (13)$$

$$CpFe(MeCN)_3^+ \longrightarrow \dot{C}pFe(MeCN)_3^{2+} + e^- \quad (14)$$

$$\dot{C}pFe(MeCN)_3^{2+} + 3MeCN \longrightarrow \dot{C}p + Fe(MeCN)_6^{2+} \quad (15)$$

Scheme 4. Eqs. (12), (13): Reaction sequence of photolysis of **CpFe(η^6-*p*-xyl)$_3^+$** in acetonitrile. Eq. (14): Electrochemical reaction of electroactive species generated during the photolysis. Eq. (15): Chemical reaction of the electrochemically generated species.

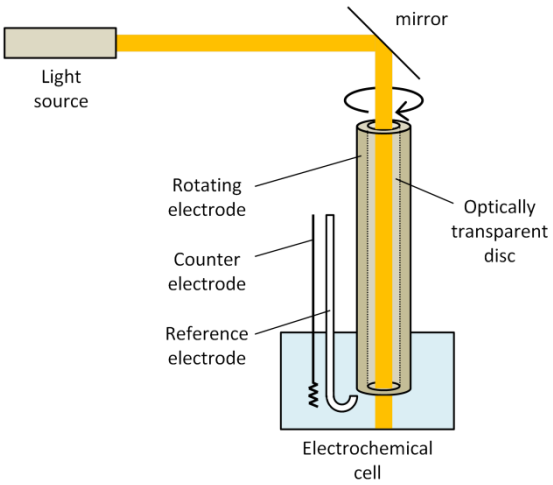

Figure. 2. A typical setup of the rotating photoelectrode technique.

2.3. Photomodulation voltammetry

Photomodulation voltammetry (PMV) [52-62] was developed by Wayner and coworkers in 1986. This system increases the sensitivity of electrochemical detection under photoirradiation by adopting the modulation principle in electrochemical measurements. In a typical setup, an electrochemical cell composed of a three-electrode configuration is used. A flashlight is used as a light source to create a transient population of the unstable species to be investigated within the electrochemical cell (Fig. 3). Wayner and coworkers succeeded in directly determining the redox potentials of some transient free radicals by using this system. [52-57] In their studies, short-lived transient species such as radicals were produced by photolysis by using a flash lamp, and voltammograms were measured. Notably, the PMV system can detect the redox current of short-lived transient species at low concentration. The shape of a voltammogram measured by PMV is typically sigmoidal with a defined diffusion-limited plateau, and the redox potentials of the transient species are determined from the voltammogram. Additionally, Wayner and coworkers analyzed the results of their experiments by digital simulation, and the lifetime of the short-lived transient species and the rate of the electron transfer were successfully obtained. [56]

Subsequently, PMV was started to be used to determine the redox potentials of photoexcited molecules. Fox and coworker used the PMV system to determine the oxidation and reduction potentials of metal complexes in photo-excited states. [61] The excited metal-to-ligand charge-transfer states of several ruthenium polypyridyl complexes (**$[RuL_3]^{2+}$ L** = 2,2'-bipyridine (**bpy**), 4,4'-dimethyl-2,2'-bipyridine (**dmb**), phenanthroline (**phen**), or bipyrazine (**bpz**)) (Scheme 5) were analyzed. Linear sweep voltammetry of these compounds was performed with the PMV system. The current in the voltammetry showed a sigmoidal shape with a defined diffusion-limited plateau, and the redox potentials of the corresponding excited states were obtained. The redox potentials obtained in this analysis were roughly consistent with the excited-state potentials of these compounds calculated from the Rehm-Weller equation [66]. A similar investigation was also performed with two organic triplet states (anthracene and triphenylene).

$$[RuL_3]^{2+} \xrightarrow{h\nu} [RuL_3]^{2+*} \quad (16)$$

$$[RuL_3]^{2+*} \longrightarrow [RuL_3]^{3+} + e^- \quad (17)$$

$$[RuL_3]^{2+*} + e^- \longrightarrow [RuL_3]^{+} \quad (18)$$

Scheme 5. Photoexcitation of **$[RuL_3]^{2+}$** and redox reaction of **$[RuL_3]^{2+}$***.

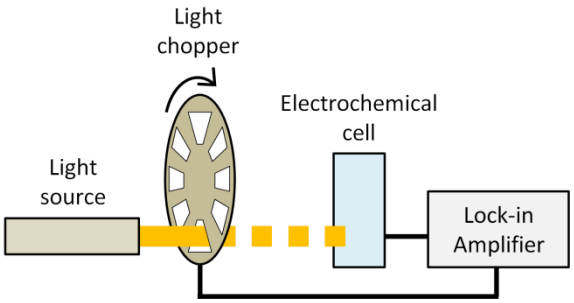

Figure. 3. A typical setup of photomodulation voltammetry.

3. Aim of this thesis

As described above, several photoelectrochemical systems have been developed to measure the electrochemical responses of a solution under photoirradiation. To further expand this research area, a system to measure cyclic voltammetry, which is one of most commonly used electrochemical methods in recent years, under photoirradiation should be developed. However, the cyclic voltammograms of solutions under photoirradiation by using the previously developed systems, *i.e.*, photopolarography, the rotating photoelectrode technique and photomodulation voltammetry, have rarely been reported.

In this thesis, the author aimed to develop a novel photoelectrochemical system for *in-situ* cyclic voltammetry under photoirradiation. The author assumed that the lack of reports is because the previously reported systems have limitations that make them unsuitable for cyclic voltammetry, which requires a quiescent solution under diffusion-limited mass transfer: in photopolarography, the solution near the surface of the electrode is not fully illuminated because the drop shadows the side opposite the lamp, in the rotating photoelectrode technique, the forced convection of the solution occurs near the surface of the electrode, and in photomodulation voltammetry, the light is irradiated intermittently. Thus we started with the development of experimental technique that can afford such diffusion-limited conditions even under photoirradiation.

4. Survey of this thesis

Chapter 1 describes the development of a novel photoelectrochemical system to perform cyclic voltammetry on a photoirradiated solution. The investigation started by measuring cyclic voltammograms of ferrocene (**Fc**), $Fe(C_5H_5)_2$, under photoirradiation. A custom-made electrochemical cell (Fig. 4) was used for measurements. **Fc** exhibits reversible redox behavior in various electrochemical conditions and is a photochemically inactive metal complex. Therefore, the electrochemical properties of **Fc** are expected to be unchanged upon photoirradiation. However, the shape of cyclic voltammogram drastically changed from a reversible wave to a sigmoidal shape under photoirradiation. Moreover, a sigmoidal-shaped voltammogram was obtained even under light that could not be absorbed by **Fc** ($\lambda > 570$ nm). These observations strongly indicate that the changes in the cyclic voltammograms did not originate from the photochemical reaction of **Fc**. Therefore, it is reasonable to presume that the photoirradiation generates convection due to local increases in temperature, and the mass transfer subsequently induced by this convection affected the electrochemical response. On the basis of the above results, the author examined several systems to decrease the current change under photoirradiation, and found that fast scanning and thin layer voltammetry suppressed the aforementioned unfavorable current change under photoirradiation.

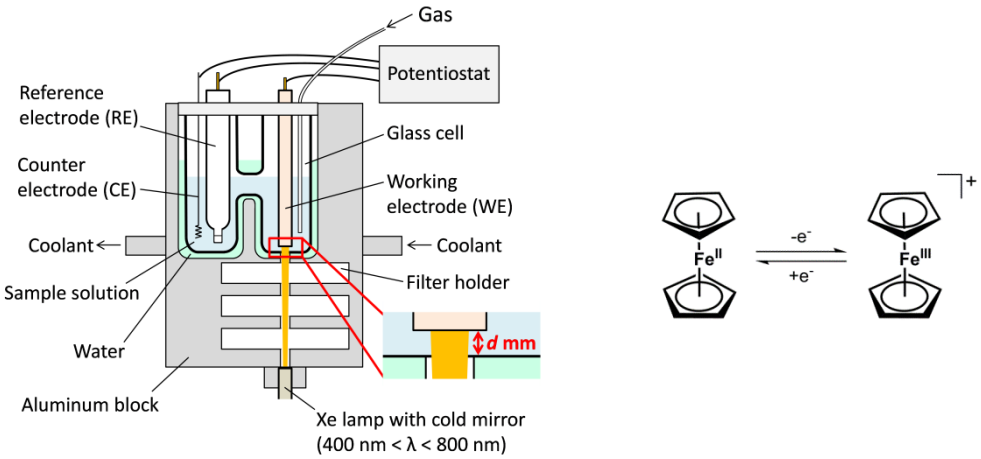

Figure. 4. The setup of thin layer voltammetry under photoirradiation.

As a further extension of the study, in Chapter 2, several attempts were performed to determine the redox potentials of a well-known metal-complex-based dye, tris(2,2'-bipyridyl)ruthenium(II) (**[Ru(bpy)$_3$]$^{2+}$**). The thin layer voltammetric system was used in this study because it allows both the precise determination of redox potentials and the detection of redox species that exhibit slow electron transfer. In the voltammogram measured under photoirradiation, a broad peak appeared at approximately +0.8 V *vs*. SCE (Fig. 5), and the potential of the peak was similar to the reported value of the reduction potential of **[Ru(bpy)$_3$]$^{2+}$***. Moreover, the intensity of the peak drastically decreased under an O_2 atmosphere and was recovered by Ar bubbling. These results indicate that the peak originated from the triplet excited species of **[Ru(bpy)$_3$]$^{2+}$**, **[Ru(bpy)$_3$]$^{2+}$*** because this species is known to be quenched by triplet dioxygen.

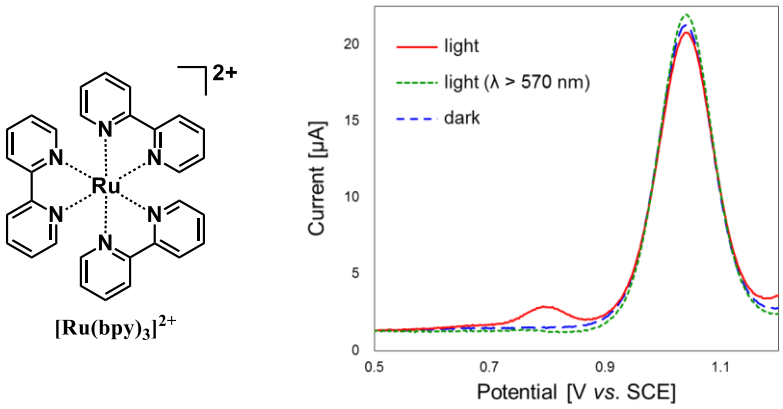

Figure. 5. Square wave voltammograms of **[Ru(bpy)$_3$]$^{2+}$** with and without photoirradiation.

Chapter 3 describes the investigation of the electrochemical response of a catalytic system under photoirradiation to detect the intermediates during the photocatalysis. The electrochemical CO_2 reduction reaction catalyzed by *meso*-tetraphenylporphyrin iron(III) chloride (**Fe(tpp)Cl**) [63, 64] was selected as a targeted reaction system, and the influence of photoirradiation on the catalytic reaction was analyzed by thin layer voltammetry. In the cyclic voltammogram of **Fe(tpp)Cl** under an Ar atmosphere, three reversible reduction waves were observed at −0.6, −1.5 and −2.1 V *vs.* ferrocenium/ferrocene (Fc^+/Fc) (Fig. 6, black solid line). Under a CO_2 atmosphere in dark conditions, a new anodic peak at approximately E_{pa} = −1.7 V was observed (Fig. 6, blue dashed line) and was assigned as the oxidative Fe–CO reassociation, a side reaction of the catalytic reaction. The intensity of the irreversible wave dramatically decreased upon photoirradiation (Fig. 6, red solid line). Under photoirradiated conditions, the photoinduced decarbonylation reaction of **[Fe^{II}(tpp)-CO]** proceeded to regenerate **[Fe^{II}(tpp)]**. Subsequently, the regenerated **[Fe^{II}(tpp)]** was reduced to **[Fe^{I}(tpp)]** at the electrode. As a result, the irreversible wave attributed to the side reaction was offset by the current attributed to the reduction of **[Fe^{II}(tpp)]**. In other words, the product formed by the side reaction in the catalytic system was smoothly converted by photoirradiation, and the electrochemical response attributed to this photoreaction was successfully observed.

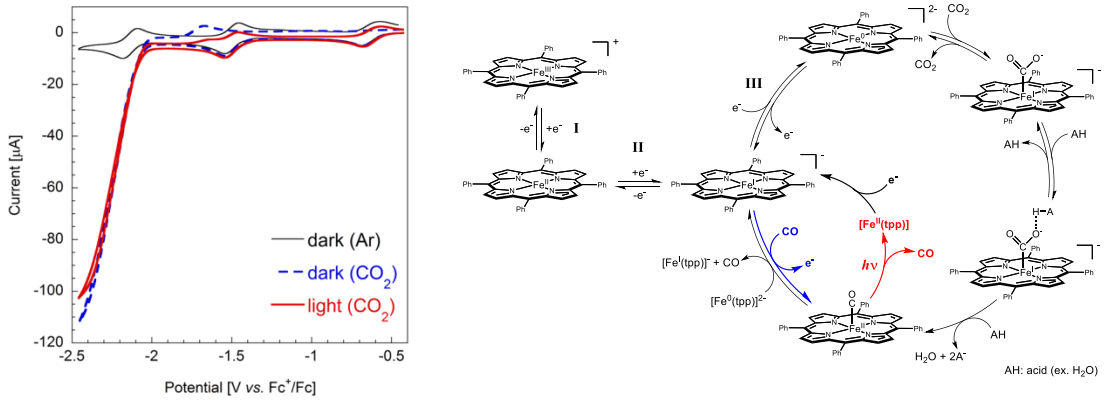

Figure. 6. Cyclic voltammograms of **Fe(tpp)Cl** with and without photoirradiation under a CO_2 atmosphere (right) and reaction mechanism of CO_2 reduction by **Fe(tpp)Cl**.

References

1. G. J. Kavarnos, N. J. Turro, Photosensitization by reversible electron transfer: theories, experimental evidence, and examples, Chem. Rev. 86 (1986) 401–449.

2. Y. Inoue, Asymmetric photochemical reactions in solution, Chem. Rev. 92 (1992) 741–770.

3. F. Bernardi, M. Olivucci, M. A. Robb, Potential energy surface crossings in organic photochemistry, Chem. Soc. Rev. 25 (1996) 321–328.

4. A. Juris V. Balzani, F. Barigelletti, S. Campagna, P. Belser, A. V. Zelewsky, Ru(II) polypyridine complexes: photophysics, photochemistry, eletrochemistry, and chemiluminescence, Coord. Chem. Rev. 84 (1988) 85–277.

5. V. Balzani, A. Juris, M. Venturi, S. Campagna, S. Serroni, Luminescent and redox-active polynuclear transition metal complexes, Chem. Rev. 96 (1996) 759–833.

6. J.-P. Sauvage, J.-P. Collin, J.-C. Chambron, S. Guillerez, C. Coudret, V. Balzani, F. Barigelletti, L. D. Cola, L. Flamigni, Ruthenium(II) and osmium(II) bis(terpyridine) complexes in covalently-linked multicomponent systems: synthesis, electrochemical behavior, absorption spectra, and photochemical and photophysical properties, Chem. Rev. 94 (1994) 993–1019.

7. J. Barber, Photosynthetic energy conversion: natural and artificial, Chem. Soc. Rev. 38 (2009) 185–196.

8. G. H. Krause, E. Weis, Chlorophyll fluorescence and photosynthesis: the basics, Annu. Rev. Plant Physiol. Plant Mol. Biol. 42 (1991) 313–349.

9. E. N. Pugh Jr., T. D. Lamb, Phototransduction in vertebrate rods and cones: molecular

mechanisms of amplification, recovery and light adaptation, in: D. G. Stavenga, W. J. DeGrip, E. N. Pugh Jr. (Eds.), Handbook of Biological Physics, vol. 3, Elsevier Science B.V., Amsterdam, 2000, pp. 183–255.

10. K.-W. Yau, R. C. Hardie, Phototransduction motifs and variations, Cell 139 (2009) 246–264.

11. D. G. Nocera, The artificial leaf, Acc. Chem. Res. 45 (2012) 767–776.

12. D. Gust, T. A. Moore, A. L. Moore, Solar fuels via artificial photosynthesis, Acc. Chem. Res. 42 (2009) 1890–1898.

13. A. Kudo, Y. Miseki, Heterogeneous photocatalyst materials for water splitting, Chem. Soc. Rev. 38 (2009) 253–278.

14. L. Fenno, O. Yizhar, K. Deisseroth, The development and application of optogenetics, Annu. Rev. Neurosci. 34 (2011) 389–412.

15. K. Deisseroth, Optogenetics, Nat. Methods 8 (2011) 26–29.

16. (a) A. Hagfeldt, G. Boschloo, L. Sun, L. Kloo, H. Pettersson, Dye-sensitized solar cells, Chem. Rev. 110 (2010) 6595–6663. (b) R. Abe, Recent progress on photocatalytic and photoelectrochemical water splitting under visible light irradiation, J. Photochem. Photobiol. C: Photochem. Rev. 11 (2010) 179–209.

17. Z. Yu, F. Li, L. Sun, Recent advances in dye-sensitized photoelectrochemical cells for solar hydrogen production based on molecular components, Energy Environ. Sci. 8 (2015) 760–775.

18. (a) L. Bertoluzzi, L. Badia-Bou, F. Fabregat-Santiago, S. Gimenez, J. Bisquert, Interpretation of cyclic voltammetry measurements of thin semiconductor films for

solar fuel applications, J. Phys. Chem. Lett. 4 (2013) 1334−1339. (b) S. Kawasaki, R. Takahashi, T. Yamamoto, M. Kobayashi, H. Kumigashira, J. Yoshinobu, F. Komori, A. Kudo, M. Lippmaa, Photoelectrochemical water splitting enhanced by self-assembled metal nanopillars embedded in an oxide semiconductor photoelectrode, Nat. Commun. 7 (2016) 11818.

19. W. R. LaCourse, I. S. Krull, Photoelectrochemical detection in analytical chemistry, Trends Anal. Chem. 4 (1985) 118–124.

20. H. Berg, Photokinetische ströme in der polarographie, Naturwissenschaften 47 (1960) 320–321.

21. H. Berg, Photopolarographie, Collect. Czech. Chem. Commun. 25 (1960) 3404.

22. H. Berg, H. Schweiss, Radikalbestimmung durch photopolarographie, Naturwissenschaften 47 (1960) 513.

23. H. Berg, H. Schweiss, Photo-polarography with a flash-lamp, Nature 191 (1961) 1270–1272.

24. H. Berg, Instabile zwischenprodukte der polarographischen, katalytischen und photosensibilisierten reduktion von benzil, Naturwissenschaften 48 (1961) 100–101.

25. H. Berg, Photopolarographische effekte durch blitzbestrahlung, Naturwissenschaften 49 (1962) 11.

26. H. Berg, Grundlagen and möglichkeiten der photo-polarographie, Rev. Polarography 11 (1963) 29–35.

27. H. Berg, H. Schweiss, Primäreffekte in der photo-polarographie, Electrochim. Acta 9 (1964) 425–430.

28. H. Berg, Photo-polarographie: XX. Systematik und problematik, J. Electroanal. Chem. Interfacial Electrochem. 15 (1967) 415–450.

29. H. Berg, On three hypotheses in photo-polarography, Electrochim. Acta 13 (1968) 1249–1252.

30. H. Berg, P. Reissmann, Photo-polarographie: XXIII. Mitt. über die ursachen von photo-restströmen, J. Electroanal. Chem. Interfacial Electrochem. 24 (1970) 427–434.

31. H. Berg, Photopolarographic aspects in photodynamic effects, J. Electroanal. Chem. Interfacial Electrochem. 65 (1975) 129–139.

32. H. Berg, Selected contributions to polarography by the bioelectrochemistry laboratory at Jena, Rev. Polarography 49 (2003) 37–61.

33. K. Yamashita, H. Imai, Studies on photo-polarography. I. Polarographic behavior of trioxalato-ferrate (III) ion under ultraviolet iradiation, Bull. Chem. Soc. Jpn. 41 (1968) 1339–1343.

34. K. Yamashita, H. Imai, Studies on photo-polarography. VI. Photo-catalytic current of chloranil at DME, Rev. Polarography 18 (1972) 10–16.

35. S. P. Perone, J. R. Birk, Application of electroanalytical techniques to the study of flash photolysis processes, Anal. Chem. 38 (1966) 1589–1593.

36. J. R. Birk, S. P. Perone, Electrochemical studies of rapid photolytic processes. A theoretical and experimental evaluation of potentiostatic analysis in flash photolyzed solutions, Anal. Chem. 40 (1968) 496–500.

37. H. E. Stapelfeldt, S. P. Perone, Photo-electrochemical behavior of benzil.

Potentiostatic monitoring following flash photolysis, Anal. Chem. 41 (1969) 628–632.

38. J. I. H. Patterson, S. P. Perone, Simultaneous electrochemical and photometric monitoring of intermediates generated by flash photolysis, Anal. Chem. 44 (1972) 1978–1982.

39. R. A. Jamieson, S. P. Perone, Electroanalytical measurements of flash-photolyzed ferrioxalate, J. Phys. Chem. 76 (1972) 830–839.

40. G. L. Kirschner, S. P. Perone, New experimental design for electroanalytical study of flash photolysis processes, Anal. Chem. 44 (1972) 443–451.

41. J. I. H. Patterson, S. P. Perone, Spectrophotometric and electrochemical studies of flash-photolyzed trioxalatoferrate (III), J. Phys. Chem. 77 (1973) 2437–2440.

42. S. S. Fratoni Jr., S. P. Perone, Studies in photoelectrochemistry: a theoretical model for induced charging currents in potentiostatic chronoamperometry, Anal. Chem. 48 (1976) 287–295.

43. D. C. Johnson, E. W. Resnick, Rotating photoelectrode for electrochemical study of the products of photochemical reactions, Anal. Chem. 44 (1972) 637–640.

44. J. R. Lubbers, E. W. Resnick, P. R. Gaines, D. C. Johnson, Digital simulation of a rotating photoelectrode. Photolysis of benzophenone in alkaline media, Anal. Chem. 46 (1974) 865–873.

45. P. R. Gaines, V. E. Peacock, D. C. Johnson, Application of a rotating photoelectrode to a photochemical study of fluorenol, Anal. Chem. 47 (1975) 1373–1379.

46. D. C. Boyd, D. A. Bohling, K. R. Mann, Application of the rotating photoelectrode to the detection of an organotransition-metal intermediate. Photoelectrochemical

detection of (η^5-C_5H_5)Fe(CH_3CN)$_3^+$, J. Am. Chem. Soc. 107 (1985) 1641–1644.

47. W. J. Albery, M. D. Archer, N. J. Field, A. D. Turner, Photochemical generation of semiquinone intermediates at a rotating semi-transparent disc electrode, Faraday Discuss. Chem. Soc. 56 (1973) 28–40.

48. W. J. Albery, M. D. Archer, R. G. Egdell, The semitransparent rotating disc electrode, J. Electroanal. Chem. Interfacial Electrochem. 82 (1977) 199–208.

49. W. J. Albery, P. N. Bartlett, W. R. Bowen, F. S. Fisher, A. W. Foulds, Photogalvanic cells: Part X. The transparent disc electrode and the iron-thionine system, J. Electroanal. Chem. Interfacial Electrochem. 107 (1980) 23–35.

50. W. J. Albery, W. R. Bowen, F. S. Fisher, A. D. Turner, Photogalvanic cells: Part VIII. The theory of the transparent rotating disc electrode, J. Electroanal. Chem. Interfacial Electrochem. 107 (1980) 1–9.

51. W. J. Albery, W. R. Bowen, F. S. Fisher, A. D. Turner, Photogalvanic cells: Part IX. Investigations using the transparent rotating disc electrode, J. Electroanal. Chem. Interfacial Electrochem. 107 (1980) 11–22.

52. D. D. M. Wayner, D. Griller. Oxidation and reduction potentials of transient free radicals, J. Am. Chem. Soc. 107 (1985) 7764–7765.

53. D. D. M. Wayner, J. J. Dannenberg, D. Griller. Oxidation potentials of α-aminoalkyl radicals: bond dissociation energies for related radical cations, Chem. Phys. Lett. 131 (1986) 189–191.

54. D. D. M. Wayner, D. J. McPhee, D. Griller. Oxidation and reduction potentials of transient free radicals, J. Am. Chem. Soc. 110 (1988) 132–137.

55. B. A. Sim, D. Griller, D. D. M. Wayner, Reduction potentials for substituted benzyl radicals: pK_a values for the corresponding toluenes, J. Am. Chem. Soc. 111 (1989) 754–755.

56. T. Nagaoka, D. Griller, D. D. M. Wayner, Digital simulation of photomodulation voltammograms: reactivity of the diphenylmethyl carbanion and carbocation in acetonitrile, J. Phys. Chem. 95 (1991) 6264–6270.

57. D. D. M. Wayner, A. Houmam, Redox properties of free radicals, Acta Chem. Scand. 52 (1998) 377–384.

58. T. Brinck, A. G. Larsen, K. M. Madsen, K. Daasbjerg, Solvation of carbanions in organic solvents: a test of the polarizable continuum model, J. Phys. Chem. B 104 (2000) 9887–9893.

59. A. G. Larsen, A. H. Holm, M. Roberson, K. Daasbjerg, Substituent effects on the oxidation and reduction potentials of phenylthiyl radicals in acetonitrile, J. Am. Chem. Soc. 123 (2001) 1723–1729.

60. T. Lund, D. D. M. Wayner, M. Jonsson, A. G. Larsen, K. Daasbjerg, Oxidation potentials of α-hydroxyalkyl radicals in acetonitrile obtained by photomodulated voltammetry, J. Am. Chem. Soc. 123 (2001) 12590–12595.

61. W. E. Jones Jr., M. A. Fox, Determination of excited-state redox potentials by phase-modulated voltammetry, J. Phys. Chem. 98 (1994) 5095–5099.

62. N. Oda, K. Tsuji, A. Ichimura, Voltammetric measurements of redox potentials of photo-excited species, Anal. Sci. 17 (2001) i375–i378.

63. I. Bhugun, D. Lexa, J.-M. Savéant, Ultraefficient selective homogeneous catalysis of the electrochemical reduction of carbon dioxide by an iron(0) porphyrin associated

with a weak Brønsted acid cocatalyst, J. Am. Chem. Soc. 116 (1994) 5015–5016.

64. C. Costentin, S. Drouet, G. Passard, M. Robert, J.-M. Savéant, Proton-coupled electron transfer cleavage of heavy-atom bonds in electrocatalytic processes. cleavage of a C−O bond in the catalyzed electrochemical reduction of CO_2, J. Am. Chem. Soc, 135 (2013) 9023–9031.

Chapter 1

Development of *in-situ* cyclic voltammetry under photoirradiation

1. Introduction

Photochemical reactions of molecular compounds have been widely studied due to their future potential applications such as artificial photosynthesis as well as their fundamental importance in chemistry. To understand the mechanisms of photochemical reactions, analysis of intermediates generated during the reactions is essential. In this context, *in-situ* electrochemical analysis of molecular substrates under photoirradiation can be a powerful technique to investigate the photochemical reaction mechanisms. As mentioned in General Introduction, there have been many reports on photoelectrochemical systems that can measure the electrochemical responses of molecular substrates in a homogeneous solution under photoirradiation, *i.e.*, photopolarography [1-24], the rotating photoelectrode technique [1,25-33] and photomodulation voltammetry [34-44]. However, cyclic voltammetry under photoirradiation by using these photoelectrochemical techniques have rarely been demonstrated, although cyclic voltammetry is one of most commonly used electrochemical methods in recent years to evaluate electronic structures of molecular substrates.

In this chapter, the author reports a novel photoelectrochemical system for *in-situ* cyclic voltammetry under photoirradiation. To investigate the reason why *in-situ* cyclic voltammetry under photoirradiation is difficult, we used a photochemically inactive metal complex as a molecular substrate, and performed *in-situ* cyclic voltammetry under photoirradiation. As a result, we found experimental conditions that can afford a quiescent solution under diffusion-limited mass transfer, which is required for measurements of cyclic voltammetry, even under photoirradiation.

2. Results

Electrochemical measurements were performed using a custom-made electrochemical cell with coolant to maintain the temperature of the sample solution during the measurement (Fig. 1). Ferrocene (**Fc**), which exhibits reversible redox behavior in various electrochemical conditions [45] and is a photochemically inactive metal complex, was adopted as a redox probe. The electrochemical properties of **Fc** are expected to be unchanged upon photoirradiation because the lifetime of the photoexcited triplet state of **Fc** is quite short (0.6 ns) [46]. Thus, the influence of the side effects induced by photoirradiation can be extracted from the electrochemical measurements of **Fc** under photoirradiation.

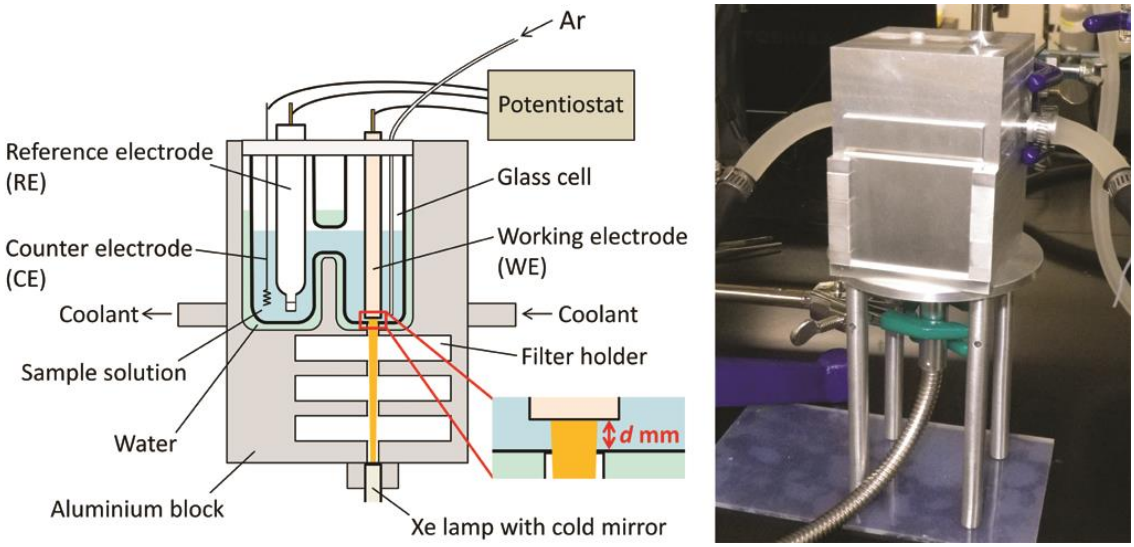

Figure 1 Custom-made photoelectrochemical cell. Schematic illustration (left) and a photograph (right) are shown. The coolant was set to 20 °C to maintain a constant sample temperature during measurement. *d* indicates the thickness of the solution layer.

The electrochemical behavior of **Fc** in acetonitrile under photoirradiation by a Xe lamp with a CM-1 cold mirror (400–800 nm) was investigated by cyclic voltammetry (CV) and chronoamperometry. Figure 2a shows the cyclic voltammograms of **Fc** with and without light irradiation. The reversible wave attributed to the redox process between **Fc** and ferrocenium ($\mathbf{Fc}^+$) was observed without light irradiation. In contrast, under photoirradiation, the peak shape became sigmoidal, and the limiting current was observed. In chronoamperometry at +0.2 V (*vs.* Fc^+/Fc), an increase in current was observed repeatedly upon photoirradiation (Fig. 2b).

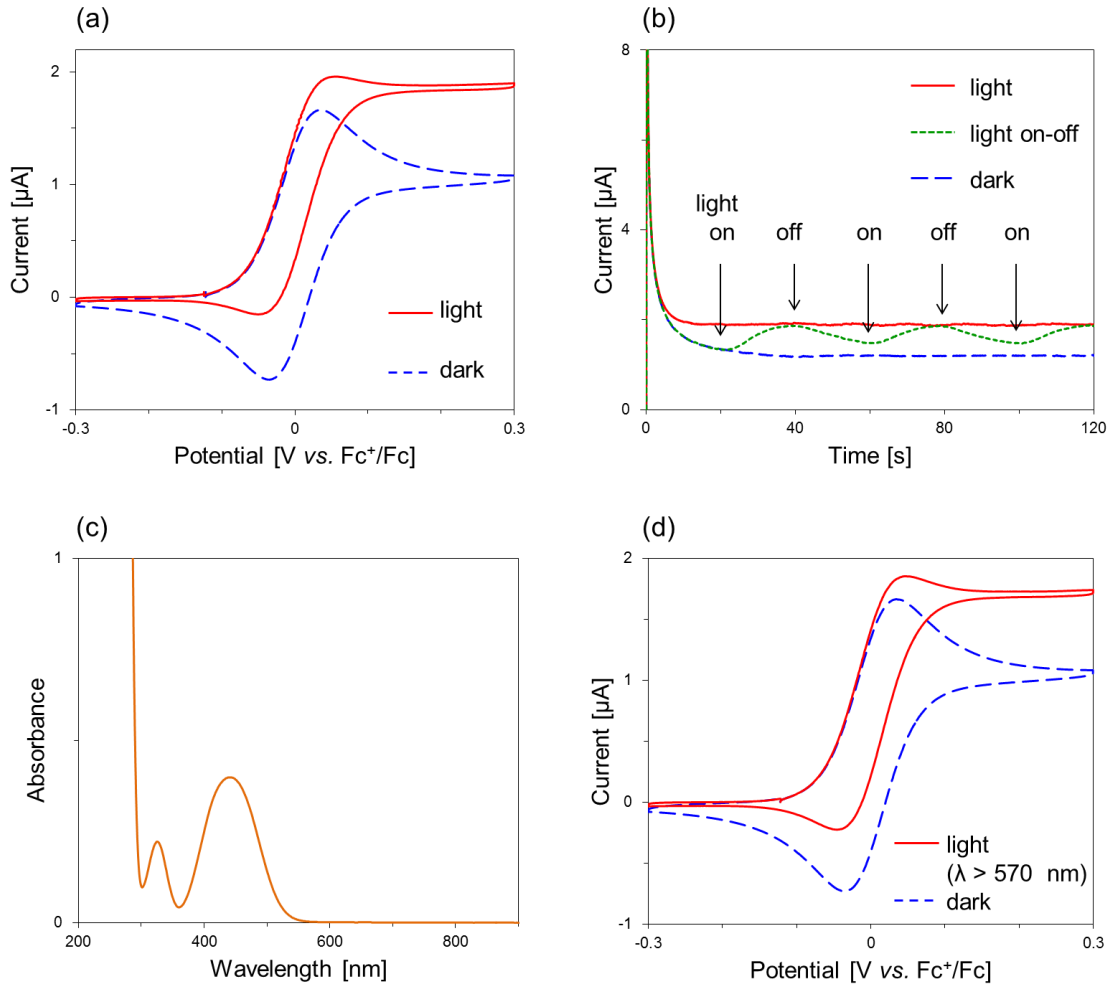

Figure 2 Relationship between the optical properties of **Fc** and the electrochemical response. (a) Cyclic voltammograms of **Fc** (0.2 mM) in 0.1 M TBAP acetonitrile solution with photoirradiation (red, 400 nm < λ < 800 nm) and without photoirradiation (blue) under an Ar atmosphere (WE: GC; CE: Pt wire; RE: Ag^{+}/Ag; scan rate: 5 mV s^{-1}). (b) Current responses to photoirradiation (400 nm < λ < 800 nm) in the chronoamperograms (0.2 V vs. Fc^{+}/Fc) of **Fc** (0.2 mM) in 0.1 M TBAP acetonitrile solution under an Ar atmosphere (WE: GC; CE: Pt wire; RE: Ag^{+}/Ag). (c) UV-Vis absorption spectrum of **Fc** (4 mM) in acetonitrile. (d) Cyclic voltammograms of **Fc** (0.2 mM) in a 0.1 M TBAP acetonitrile solution under photoirradiation (red, 570 < λ < 800 nm) and in the dark (blue) under an Ar atmosphere (WE: GC; CE: Pt wire; RE: Ag^{+}/Ag; scan rate: 5 mV s^{-1}). The shapes of the cyclic voltammograms dramatically changed upon photoirradiation regardless of the irradiation wavelength.

To identify the origin of this phenomenon, the temperature of the sample solution was measured. However, a large elevation in the temperature of the solution was not observed within the timescale of the electrochemical measurements performed in this study (Fig. 3). Note that small increases in temperature do not affect the electrochemical response of **Fc** because the reversibility of the redox process is maintained at 248.15–298.15 K [47]. Therefore, a change in the global temperature of the sample solution was not the cause of the electrochemical response under photoirradiation. Subsequently, CV was performed using light that cannot be absorbed by **Fc** (λ > 570 nm, Fig. 2c). Even in this case, a sigmoidal voltammogram was also obtained, as depicted in Figure 2d, suggesting that the changes in the cyclic voltammograms were not related to the photochemical properties of **Fc**. The sigmoidal shape observed in CV under photoirradiation indicated that the diffusion layer was affected by the mass transfer induced by convection [48]. These results suggested that the photoirradiation may have generated convection due to local increases in temperature, and the mass transfer subsequently induced by this convection affected the electrochemical responses.

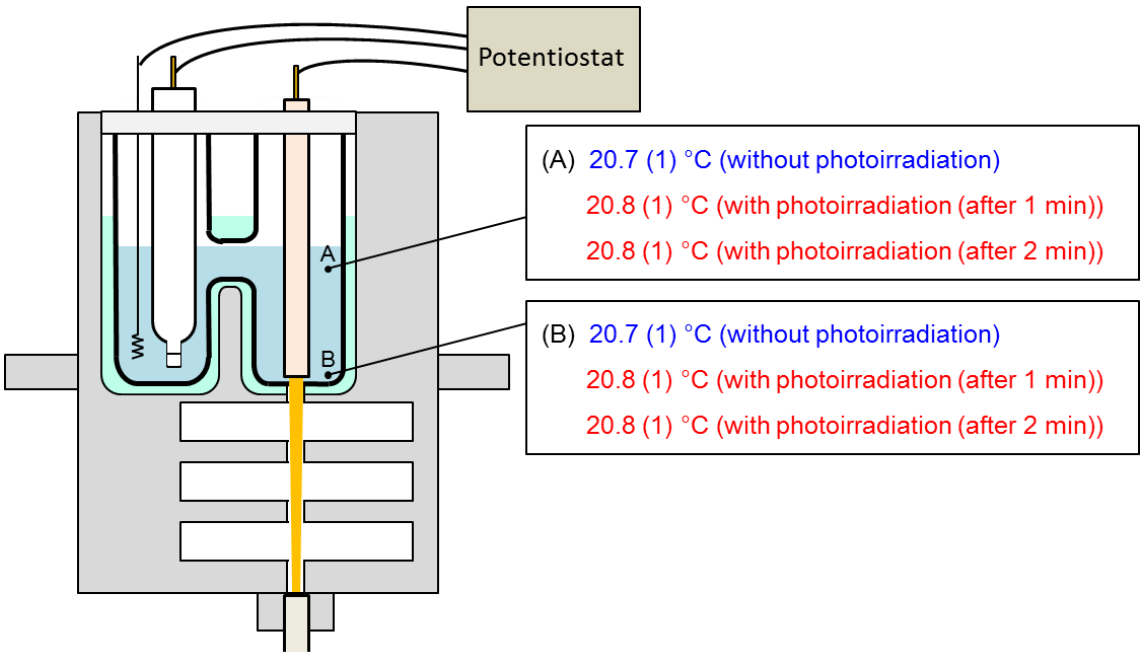

Figure 3 Temperature distribution of an acetonitrile solution containing **Fc** (0.2 mM) and TBAP (0.1 M) in the custom-made cell.

Based on the above results, we aimed to decrease the current change under photoirradiation. First, measurements were performed using a rotating disk electrode (RDE) [49] as the working electrode. RDEs can generate an extremely thin diffusion layer by forcing convection via the rotation of the electrode. In fact, upon increasing the rotating speed of the working electrode, the cyclic voltammograms under photoirradiation gradually became similar in appearance to those in the absence of photoirradiation (Fig. 4). This result indicates that the convection induced by photoirradiation was negated by the forced convection of the RDE electrode.

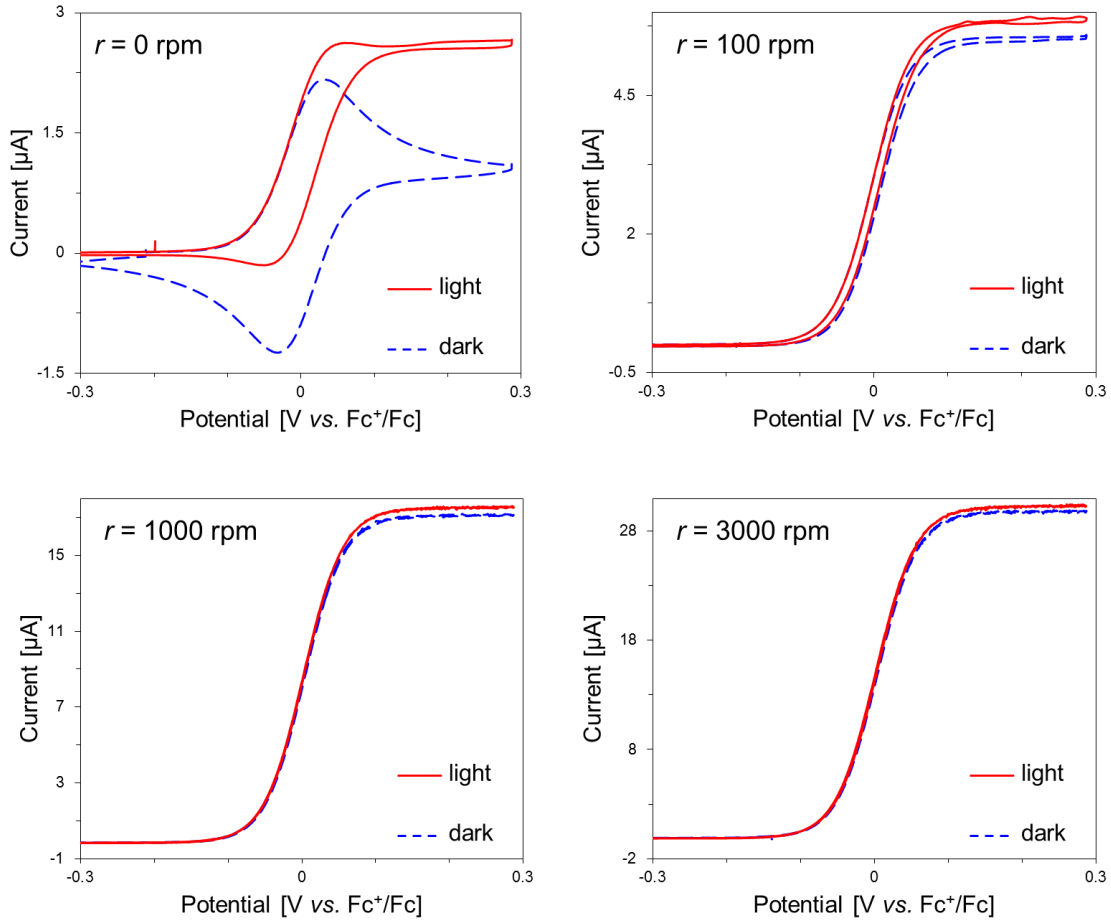

Figure 4 Cyclic voltammograms of **Fc** with various rotation speeds of RDE with and without photoirradiation. Measurements were performed in a 0.1 M TBAP acetonitrile solution under an Ar atmosphere, and the concentration of **Fc** was adjusted to 0.2 mM. The red and blue lines are the cyclic voltammograms under photoirradiation (400 nm < λ < 800 nm) and in the dark, respectively. *r* indicates the rotation speeds of the working electrode. (WE: GC; CE: Pt wire; RE: Ag^{+}/Ag; scan rate: 10 mV s^{-1}).

Next, the effect of the scan rate on the electrochemical response under photoirradiation was examined to identify more easily accessible conditions for suppressing convection. As shown in Figure 5, although a relatively fast scan rate, which is not suitable for detecting redox species that exhibit slow electron transfer, was required, the current change was effectively suppressed by increasing the scan rate. In general, the thickness of the diffusion layer (μ) changes with time (t), and μ is on the order of $\mu = (Dt)^{1/2}$ (D: diffusion coefficient) [50]. Therefore, as the scan rate increases, μ becomes small. In this situation, the mass transfer of **Fc** and $\mathbf{Fc}^+$ around the electrode is predominantly determined by the electrochemical reaction, and the effect of the convection induced by photoirradiation becomes negligible.

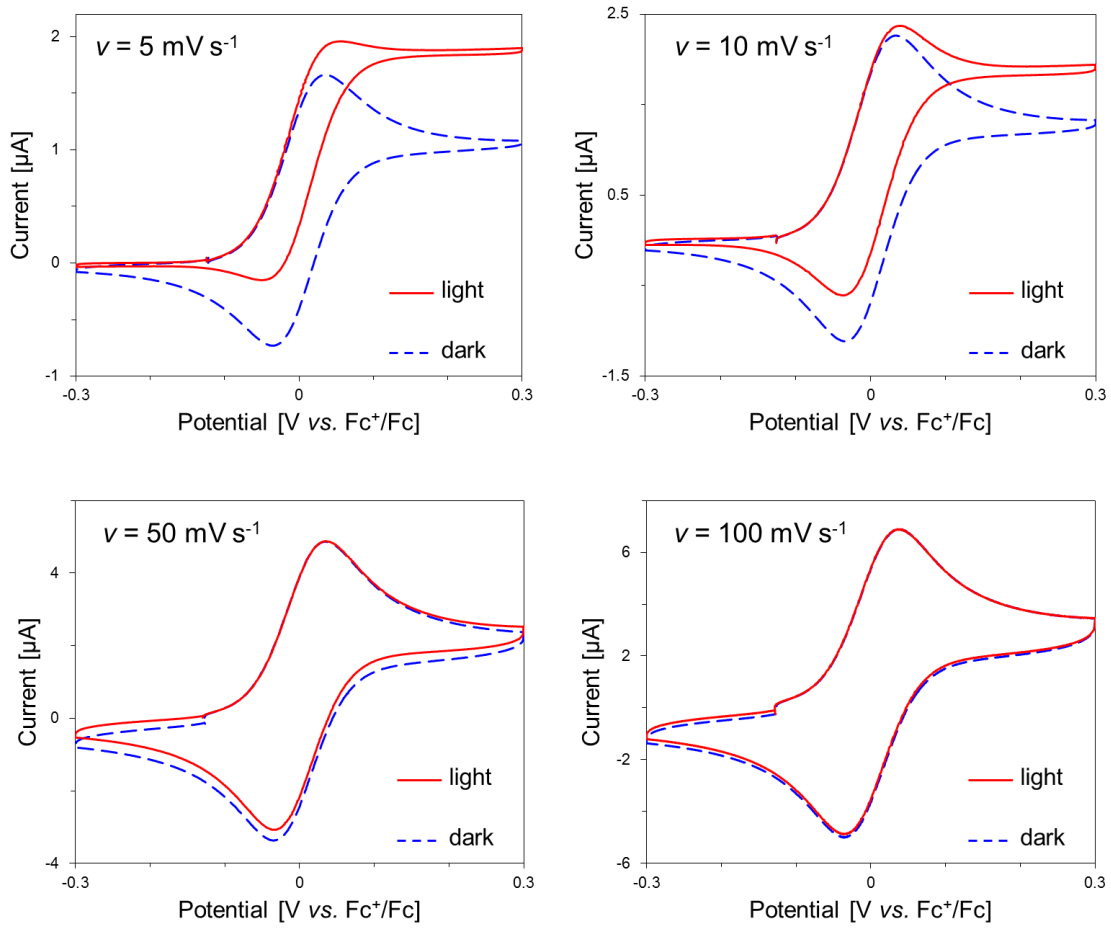

Figure 5 Dependence of the cyclic voltammograms of **Fc** on the scan rate with and without photoirradiation. Measurements were performed in a 0.1 M TBAP acetonitrile solution under an Ar atmosphere, and the concentration of **Fc** was adjusted to 0.2 mM. The red and blue lines are the cyclic voltammograms under photoirradiation (400 nm < λ < 800 nm) and in the dark, respectively. *v* indicates the scan rate of each measurement. (WE: GC; CE: Pt wire; RE: Ag^{+}/Ag).

Finally, thin layer cyclic voltammetry (TLCV) [51] was used as a simple and versatile technique to evaluate electrochemical properties under photoirradiation. This technique allows us to perform electrochemical measurements without considering the convection within a cell, and thus the effect of convection is expected to be excluded. To assess the validity of our strategy, the thickness of the solution layer (*d*, Fig. 1) was changed by adjusting the position of the working electrode. The sigmoidal-shaped voltammogram gradually changed to a reversible shape with reducing *d*, and the reversible redox wave of **Fc** was observed even at slow scan rates (5 mV s^{-1}) when *d* was smaller than 0.25 mm (Fig. 6). The similar results were observed in various solutions with the thin layer technique (Fig. 7).

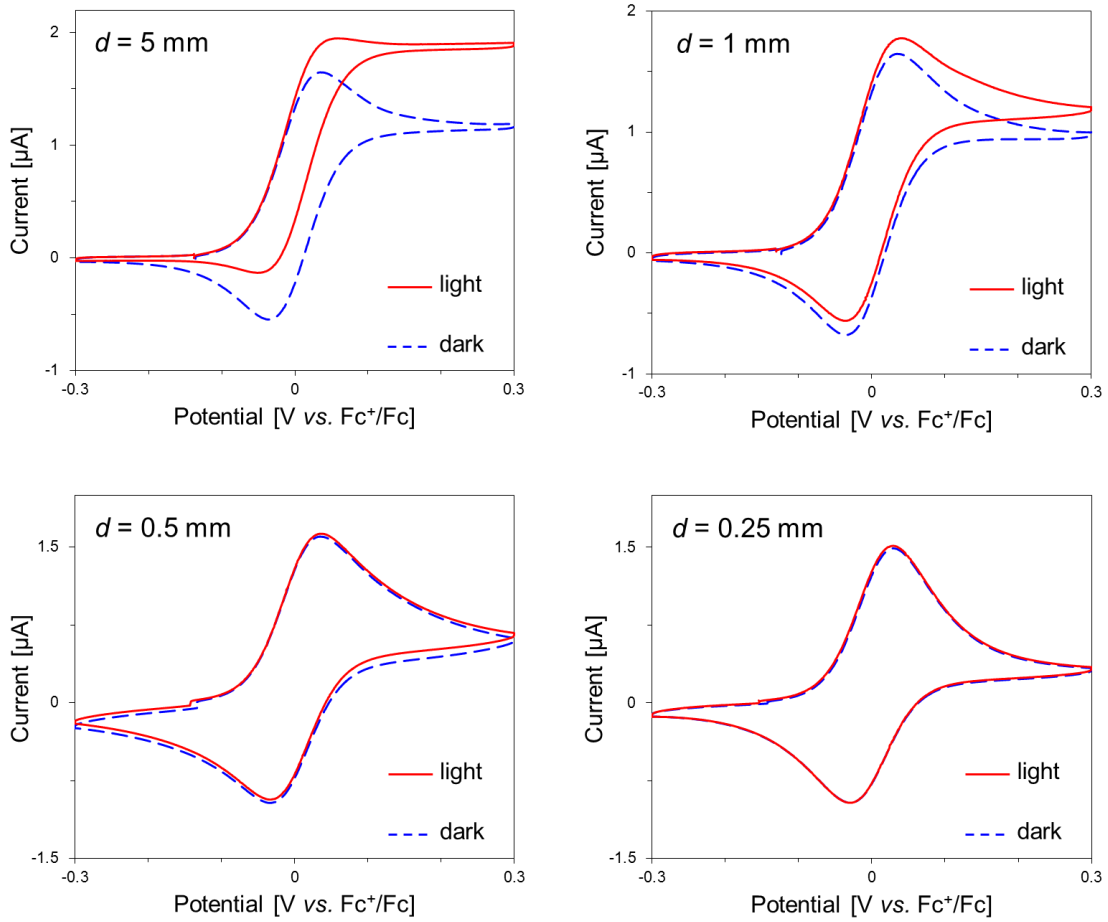

Figure 6 Dependence of the cyclic voltammograms of **Fc** on the layer thickness with and without photoirradiation. Measurements were performed in a 0.1 M TBAP acetonitrile solution under an Ar atmosphere, and the concentration of **Fc** was adjusted to 0.2 mM. The red and blue lines are the cyclic voltammograms under photoirradiation (400 nm < λ < 800 nm) and in the dark, respectively. *d* indicates the thickness of the solution layer. (WE: GC; CE: Pt wire; RE: Ag^{+}/Ag; scan rate: 5 mV s^{-1}).

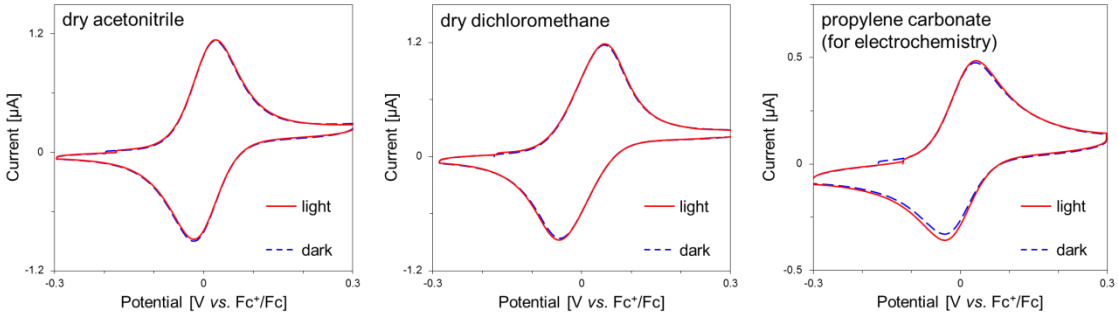

Figure 7 Thin layer cyclic voltammograms of **Fc** in various solution systems with and without photoirradiation. Measurements were performed in 0.1 M TBAP solutions under an Ar atmosphere, and the concentration of **Fc** was adjusted to 0.2 mM. The thickness of the solution layer (*d*) was 0.25 mm. The red and blue lines are the cyclic voltammograms under photoirradiation (400 nm < λ < 800 nm) and those in the dark, respectively (WE: GC; CE: Pt wire; RE: Ag^{+}/Ag; scan rate: 5 mV s^{-1}).

3. Discussions

The electrochemical measurement of homogeneous solutions under photoirradiation is difficult for numerous reasons. In cyclic voltammetry, which is most frequently used technique to determine redox potentials, the oxidation/reduction of electroactive molecule creates a concentration gradient at the electrode surface. Subsequently, the current which is proportional to concentration gradient near the electrode surface flows if the electron transfer is fast enough [50]. The redox potentials of molecules can be precisely evaluated when the concentration gradient is mainly determined by the electrochemical reaction. However, as described in the previous section, photoirradiation induces convection, and this convection generates the concentration gradient that disturbs the molecular diffusion. As a result, cyclic voltammograms become sigmoidal in shape because the electrochemical signal originating from convection, which is essentially unrelated to the properties of the molecules, dominates, and the determination of the redox potential is not possible.

To overcome this problem, the RDE technique and measurements using fast scan rates were adopted. As shown in Figures 4 and 5, we succeeded in suppressing the disturbance of mass transfer induced by convection and in collecting substantial data of electrochemical measurements under photoirradiation by thinning the diffusion layer. Additionally, the TLCV technique was also employed, and the influence of photoirradiation was found to become negligible (Fig. 6) when limiting the thickness of the solution layer to less than 0.25 mm.

4. Conclusions

The author has designed a novel photoelectrochemical system to perform cyclic voltammetry on a photoirradiated solution. Ferrocene (**Fc**), which exhibits reversible redox behavior in various electrochemical conditions and is a photochemically inactive metal complex, was adopted as a redox probe. The electrochemical measurements were performed with a custom-made photoelectrochemical cell with coolant to keep the temperature of solution. Although the electrochemical properties of **Fc** are expected to be unchanged upon photoirradiation, the shape of cyclic voltammogram drastically changed from a reversible wave to a sigmoidal shape under photoirradiation. Furthermore, the sigmoidal-shaped voltammograms were obtained even if the wavelength of the light was set to the region in which the absorption band of ferrocene does not exist. These results strongly indicate that the changes in the cyclic voltammograms did not originate from the photochemical reaction of **Fc**. Therefore, it is reasonable to presume that the photoirradiation generates convection due to local increases in temperature, and the mass transfer subsequently induced by this convection affected the electrochemical response. To overcome this problem, several systems were examined to decrease the current change under photoirradiation, and eventually found that two systems (fast scanning and thin layer voltammetry) suppressed the aforementioned unfavorable current change under photoirradiation. This novel system is an important step to develop the electrochemical analysis of molecular substrates in homogeneous solution under photoirradiation.

5. Experimental Section

5.1. Materials

Ferrocene (**Fc**) and Na_2SO_4 were purchased from Wako Pure Chemical Industries, Ltd. Acetonitrile (HPLC grade) and propylene carbonate (for electrochemistry) were purchased from the Kanto Chemical Co., Inc. Tetra(*n*-butyl)ammonium perchlorate (TBAP) was purchased from Tokyo Chemical Industry Co., Ltd. All solvents and reagents were of the highest quality available and were used as received, except for TBAP. TBAP was recrystallized from absolute ethanol and dried in vacuo. H_2O was purified using a Millipore MilliQ purifier. Dry acetonitrile and dry dichloromethane were degassed and purified under N_2 atmosphere using a GlassContour solvent system (Nikko Hansen Co., Ltd.).

5.2. Measurements

All electrochemical measurements were conducted under argon. A three-electrode configuration was employed in conjunction with a Biologic SP-50 potentiostat interfaced to a computer with Biologic EC-Lab software. The measurements were performed using the system shown in Figure 1, with the exception of the rotating disk electrode (RDE) measurements. The RDE measurements were conducted using a BAS RRDE-3A at ambient temperature, 20 °C. The photoirradiation was performed using an ILC Technology CERMAX LX-300 Xe lamp (operated at 150 W unless otherwise mentioned) equipped with a CM-1 cold mirror (400 nm < λ < 800 nm). In some experiments, an OG570 longpass filter (λ > 570 nm, from SCHOTT) was used to select a specific wavelength region for photoirradiation. In all cases, a platinum wire counter electrode (diameter 0.5 mm, from BAS) and a GC disk working electrode (diameter 3 mm, from BAS) were used. The working electrode was treated between scans by means of polishing with 0.05 μm alumina paste (from BAS) and washing with purified H_2O. For all measurements, an Ag^+/Ag reference electrode was used. The supporting electrolyte was 0.1 M TBAP. The potentials reported within these measurements were referenced to the Fc^+/Fc couple at 0 V. UV-visible absorption spectra were recorded on a SHIMADZU UV-1800 UV/Visible spectrophotometer.

References

1. W. R. LaCourse, I. S. Krull, Photoelectrochemical detection in analytical chemistry, Trends Anal. Chem. 4 (1985) 118–124.

2. H. Berg, Photokinetische ströme in der polarographie, Naturwissenschaften 47 (1960) 320–321.

3. H. Berg, Photopolarographie, Collect. Czech. Chem. Commun. 25 (1960) 3404.

4. H. Berg, H. Schweiss, Radikalbestimmung durch photopolarographie, Naturwissenschaften 47 (1960) 513.

5. H. Berg, H. Schweiss, Photo-polarography with a flash-lamp, Nature 191 (1961) 1270–1272.

6. H. Berg, Instabile zwischenprodukte der polarographischen, katalytischen und photosensibilisierten reduktion von benzil, Naturwissenschaften 48 (1961) 100–101.

7. H. Berg, Photopolarographische effekte durch blitzbestrahlung, Naturwissenschaften 49 (1962) 11.

8. H. Berg, Grundlagen and möglichkeiten der photo-polarographie, Rev. Polarography 11 (1963) 29–35.

9. H. Berg, H. Schweiss, Primäreffekte in der photo-polarographie, Electrochim. Acta 9 (1964) 425–430.

10. H. Berg, Photo-polarographie: XX. Systematik und problematik, J. Electroanal. Chem. Interfacial Electrochem. 15 (1967) 415–450.

11. H. Berg, On three hypotheses in photo-polarography, Electrochim. Acta 13 (1968) 1249–1252.

12. H. Berg, P. Reissmann, Photo-polarographie: XXIII. Mitt. über die ursachen von photo-restströmen, J. Electroanal. Chem. Interfacial Electrochem. 24 (1970) 427–434.

13. H. Berg, Photopolarographic aspects in photodynamic effects, J. Electroanal. Chem. Interfacial Electrochem. 65 (1975) 129–139.

14. H. Berg, Selected contributions to polarography by the bioelectrochemistry laboratory at Jena, Rev. Polarography 49 (2003) 37–61.

15. K. Yamashita, H. Imai, Studies on photo-polarography. I. Polarographic behavior of trioxalato-ferrate (III) ion under ultraviolet iradiation, Bull. Chem. Soc. Jpn. 41 (1968) 1339–1343.

16. K. Yamashita, H. Imai, Studies on photo-polarography. VI. Photo-catalytic current of chloranil at DME, Rev. Polarography 18 (1972) 10–16.

17. S. P. Perone, J. R. Birk, Application of electroanalytical techniques to the study of flash photolysis processes, Anal. Chem. 38 (1966) 1589–1593.

18. J. R. Birk, S. P. Perone, Electrochemical studies of rapid photolytic processes. A theoretical and experimental evaluation of potentiostatic analysis in flash photolyzed solutions, Anal. Chem. 40 (1968) 496–500.

19. H. E. Stapelfeldt, S. P. Perone, Photo-electrochemical behavior of benzil. Potentiostatic monitoring following flash photolysis, Anal. Chem. 41 (1969) 628–632.

20. J. I. H. Patterson, S. P. Perone, Simultaneous electrochemical and photometric monitoring of intermediates generated by flash photolysis, Anal. Chem. 44 (1972)

1978–1982.

21. R. A. Jamieson, S. P. Perone, Electroanalytical measurements of flash-photolyzed ferrioxalate, J. Phys. Chem. 76 (1972) 830–839.

22. G. L. Kirschner, S. P. Perone, New experimental design for electroanalytical study of flash photolysis processes, Anal. Chem. 44 (1972) 443–451.

23. J. I. H. Patterson, S. P. Perone, Spectrophotometric and electrochemical studies of flash-photolyzed trioxalatoferrate (III), J. Phys. Chem. 77 (1973) 2437–2440.

24. S. S. Fratoni Jr., S. P. Perone, Studies in photoelectrochemistry: a theoretical model for induced charging currents in potentiostatic chronoamperometry, Anal. Chem. 48 (1976) 287–295.

25. D. C. Johnson, E. W. Resnick, Rotating photoelectrode for electrochemical study of the products of photochemical reactions, Anal. Chem. 44 (1972) 637–640.

26. J. R. Lubbers, E. W. Resnick, P. R. Gaines, D. C. Johnson, Digital simulation of a rotating photoelectrode. Photolysis of benzophenone in alkaline media, Anal. Chem. 46 (1974) 865–873.

27. P. R. Gaines, V. E. Peacock, D. C. Johnson, Application of a rotating photoelectrode to a photochemical study of fluorenol, Anal. Chem. 47 (1975) 1373–1379.

28. D. C. Boyd, D. A. Bohling, K. R. Mann, Application of the rotating photoelectrode to the detection of an organotransition-metal intermediate. Photoelectrochemical detection of $(\eta^5\text{-}C_5H_5)Fe(CH_3CN)_3^+$, J. Am. Chem. Soc. 107 (1985) 1641–1644.

29. W. J. Albery, M. D. Archer, N. J. Field, A. D. Turner, Photochemical generation of semiquinone intermediates at a rotating semi-transparent disc electrode, Faraday

Discuss. Chem. Soc. 56 (1973) 28–40.

30. W. J. Albery, M. D. Archer, R. G. Egdell, The semitransparent rotating disc electrode, J. Electroanal. Chem. Interfacial Electrochem. 82 (1977) 199–208.

31. W. J. Albery, P. N. Bartlett, W. R. Bowen, F. S. Fisher, A. W. Foulds, Photogalvanic cells: Part X. The transparent disc electrode and the iron-thionine system, J. Electroanal. Chem. Interfacial Electrochem. 107 (1980) 23–35.

32. W. J. Albery, W. R. Bowen, F. S. Fisher, A. D. Turner, Photogalvanic cells: Part VIII. The theory of the transparent rotating disc electrode, J. Electroanal. Chem. Interfacial Electrochem. 107 (1980) 1–9.

33. W. J. Albery, W. R. Bowen, F. S. Fisher, A. D. Turner, Photogalvanic cells: Part IX. Investigations using the transparent rotating disc electrode, J. Electroanal. Chem. Interfacial Electrochem. 107 (1980) 11–22.

34. D. D. M. Wayner, D. Griller. Oxidation and reduction potentials of transient free radicals, J. Am. Chem. Soc. 107 (1985) 7764–7765.

35. D. D. M. Wayner, J. J. Dannenberg, D. Griller. Oxidation potentials of α-aminoalkyl radicals: bond dissociation energies for related radical cations, Chem. Phys. Lett. 131 (1986) 189–191.

36. D. D. M. Wayner, D. J. McPhee, D. Griller. Oxidation and reduction potentials of transient free radicals, J. Am. Chem. Soc. 110 (1988) 132–137.

37. B. A. Sim, D. Griller, D. D. M. Wayner, Reduction potentials for substituted benzyl radicals: pK_a values for the corresponding toluenes, J. Am. Chem. Soc. 111 (1989) 754–755.

38. T. Nagaoka, D. Griller, D. D. M. Wayner, Digital simulation of photomodulation voltammograms: reactivity of the diphenylmethyl carbanion and carbocation in acetonitrile, J. Phys. Chem. 95 (1991) 6264–6270.

39. D. D. M. Wayner, A. Houmam, Redox properties of free radicals, Acta Chem. Scand. 52 (1998) 377–384.

40. T. Brinck, A. G. Larsen, K. M. Madsen, K. Daasbjerg, Solvation of carbanions in organic solvents: a test of the polarizable continuum model, J. Phys. Chem. B, 104 (2000) 9887–9893.

41. A. G. Larsen, A. H. Holm, M. Roberson, K. Daasbjerg, Substituent effects on the oxidation and reduction potentials of phenylthiyl radicals in acetonitrile, J. Am. Chem. Soc. 123 (2001) 1723–1729.

42. T. Lund, D. D. M. Wayner, M. Jonsson, A. G. Larsen, K. Daasbjerg, Oxidation potentials of α-hydroxyalkyl radicals in acetonitrile obtained by photomodulated voltammetry, J. Am. Chem. Soc. 123 (2001) 12590–12595.

43. W. E. Jones Jr., M. A. Fox, Determination of excited-state redox potentials by phase-modulated voltammetry, J. Phys. Chem. 98 (1994) 5095–5099.

44. N. Oda, K. Tsuji, A. Ichimura, Voltammetric measurements of redox potentials of photo-excited species, Anal. Sci. 17 (2001) i375–i378.

45. G. Gritzner, J. Kuta, Recommendations on reporting electrode potentials in nonaqueous solvents, J. Pure Appl. Chem. 56 (1984) 461–466.

46. A. Maciejewski, A. Jaworska-Augustyniak, Z. Szeluga, J. Wojtczak, J. Karolczak, Determination of ferrocene triplet lifetime by measuring $T_1 \rightarrow T_1$ energy transfer to phenylosazone-D-glucose, Chem. Phys. Lett. 153 (1988) 227–232.

47. N. G. Tsierkezos, Cyclic voltammetric studies of ferrocene in nonaqueous solvents in the temperature range from 248.15 to 298.15 K, J. Solution Chem. 36 (2007) 289–302.

48. C. Renault, M. J. Anderson, R. M. Crooks, Electrochemistry in hollow-channel paper analytical devices, J. Am. Chem. Soc. 136 (2014) 4616–4623.

49. F. Opekar, P. Beran, Rotating disk electrodes, J. Electroanal. Chem. Interfacial Electrochem. 69 (1976) 1–105.

50. A. J. Bard, L. R. Faulkner, Electrochemical Methods: Fundamentals and Applications, 2nd Edition, John Wiley & Sons, Inc., New York, 2001.

51. A. T. Hubbard, Study of the kinetics of electrochemical reactions by thin-layer voltammetry: I. theory. J. Electroanal. Chem. Interfacial Electrochem. 22 (1969) 165–174.

Chapter 2

Detection of photoexcited species by *in-situ* cyclic voltammetry under photoirradiation

1. Introduction

Photoinduced electron transfer (PET) is a key process in reactions that convert light energy to electrical or chemical energy, both in natural [1,2] and artificial systems [3-5]. The efficiency of PET, which largely affects the performance of these systems, is correlated with the redox properties of the photoexcited molecule, which transfers electrons or holes during the PET reaction. Hence, determining the redox potentials of photoexcited molecules is of great significance not only for understanding the mechanisms of PET reactions but also for achieving highly efficient light-energy conversion systems. Electrochemical analysis under photoirradiation should enable the measurement of the redox potentials of excited species. However, reports of the direct electrochemical detection of photoexcited molecules have been limited to only a few examples in which specialized photoelectrochemical instrumentation was required [6,7], and the redox potentials of excited states have more commonly been indirectly estimated using the 0-0 transition energy (E_{00}) [8] or the quenching rate constant (k_q) [9,10].

As mentioned in Chapter 1, the author developed a novel photoelectrochemical system that can demonstrate *in-situ* cyclic voltammetry under photoirradiation. In this chapter, the author applied the technique to detect photoexcited species in PET reactions.

2. Results

The results described in the previous chapter encouraged us to detect photoexcited species. In this experiment, the TLCV technique was employed because this simple technique allows both the precise determination of redox potentials and the detection of redox species that exhibit slow electron transfer (vide supra). A well-known metal complex based dye, tris(2,2'-bipyridyl)ruthenium(II) (**$[Ru(bpy)_3]^{2+}$**), which is known to have an excited state (^{3}MLCT) with a long lifetime (t = 0.64 μs in water (20 °C) [11]), was adopted as the redox probe in this experiment. As shown in Figure 1a, one reversible peak, attributed to the Ru^{III}/Ru^{II} redox couple, was observed in the measurement without photoirradiation. Upon photoirradiation, the redox wave attributed to the oxidation of Ru^{II} to Ru^{III} changed to an irreversible peak, and a new broad peak appeared at approximately +0.8 V (*vs.* SCE). Note that these changes upon photoirradiation occurred only when **$[Ru(bpy)_3]^{2+}$** absorbed the irradiated light (Fig. 1), which implies that the generation of the photoexcited species of **$[Ru(bpy)_3]^{2+}$**, **$[Ru(bpy)_3]^{2+}$***, was related to these photo responses. Further analysis of this phenomenon was performed by square wave voltammetry (SWV), which can minimize the contribution from the capacitive charging current and provide voltammograms with low background. Similar to the results of CV, a new peak appeared at +0.8 V *vs.* SCE only when the wavelength of the light overlapped with the absorption band of **$[Ru(bpy)_3]^{2+}$** (Fig. 2). Furthermore, the peak appeared repeatedly in conjunction with photoirradiation (Fig. 3). It was also confirmed that the peak disappeared almost completely under an O_2 atmosphere [11], and then reproduced after Ar bubbling (Fig. 4).

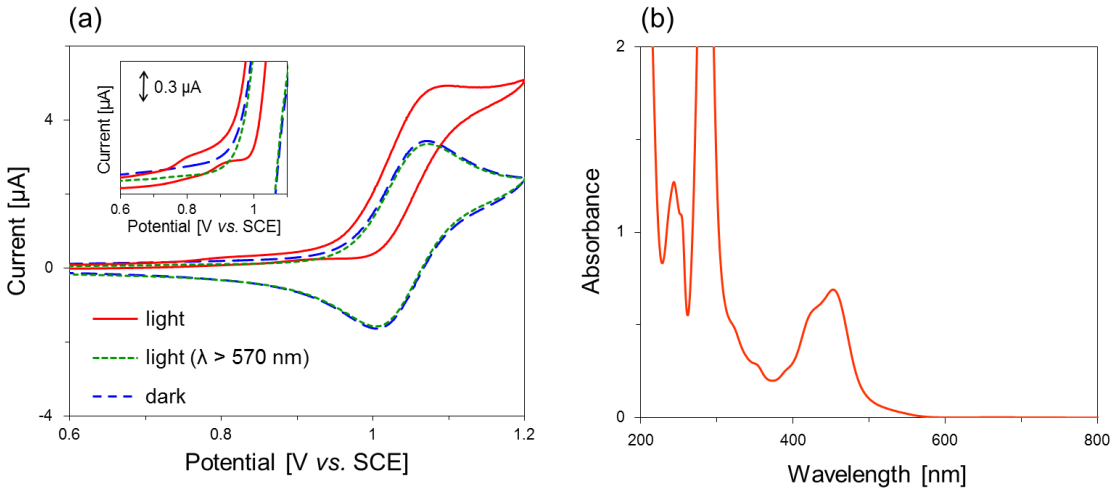

Figure 1 Relationship between the optical properties of **$[Ru(bpy)_3](NO_3)_2$** and the electrochemical response. (a) Thin layer cyclic voltammograms of **$[Ru(bpy)_3](NO_3)_2 \cdot 5H_2O$** (1 mM) in 0.1 M Na_2SO_4 aqueous solution under photoirradiation (red, 400 nm < λ < 800 nm; green, 570 nm < λ < 800 nm) and in the dark (blue) under an Ar atmosphere (WE: GC; CE: Pt wire; RE: SCE; scan rate: 5 mV s^{-1}). (b) UV-Vis absorption spectrum of **$[Ru(bpy)_3](NO_3)_2 \cdot 5H_2O$** (0.05 mM) in water. A drastic change in the shape of the cyclic voltammogram was observed when the solution was irradiated with visible light (400-800 nm).

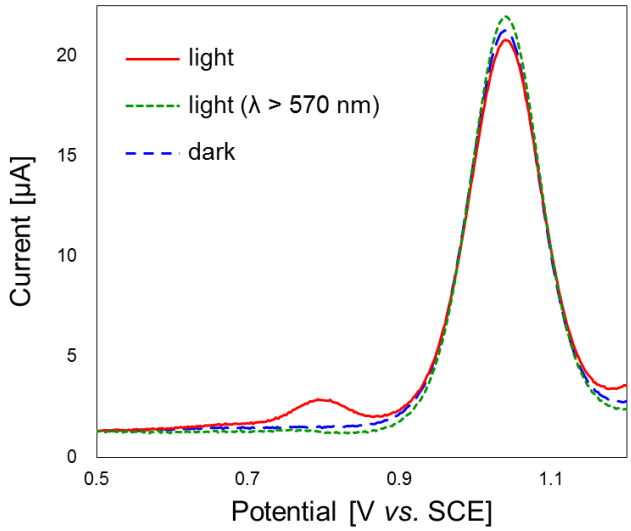

Figure 2 Thin layer square wave voltammograms of **$[Ru(bpy)_3](NO_3)_2 \cdot 5H_2O$** (1 mM) in a 0.1 M Na_2SO_4 aqueous solution under photoirradiation (red, 400 nm < λ < 800 nm; green, 570 nm < λ < 800 nm) and in the dark (blue) under an Ar atmosphere (WE: GC; CE: Pt wire; RE: SCE; scan rate: 5 mV s^{-1}). Similar to the results of CV, a new peak appeared when the sample was irradiated with visible light (400-800 nm).

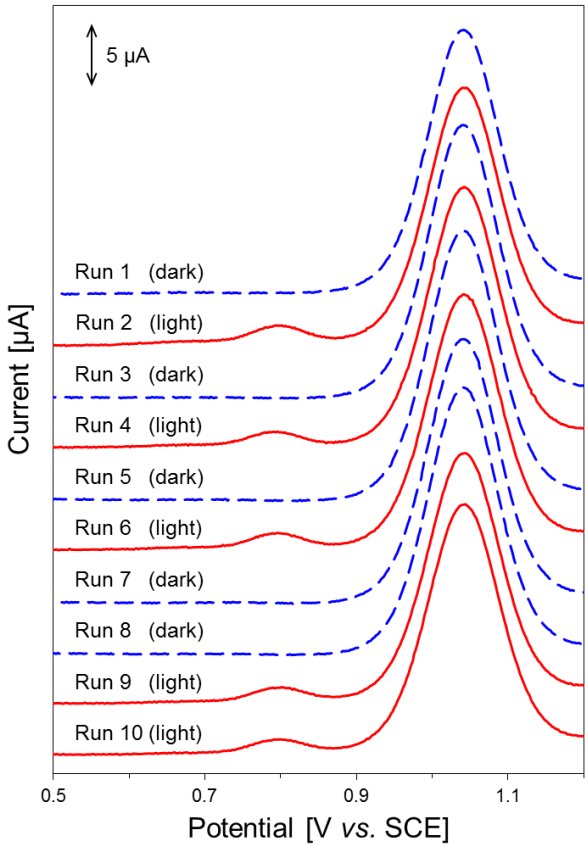

Figure 3 Thin layer square wave voltammograms of **$[Ru(bpy)_3](NO_3)_2 \cdot 5H_2O$** (1 mM) in a 0.1 M Na_2SO_4 aqueous solution under photoirradiation (red, 400 nm < λ < 800 nm) and in the dark (blue) under an Ar atmosphere (WE: GC; CE: Pt wire; RE: SCE; scan rate: 5 mV s^{-1}). The peak at approximately 0.8 V (*vs.* SCE) repeatedly appeared only when light was irradiated.

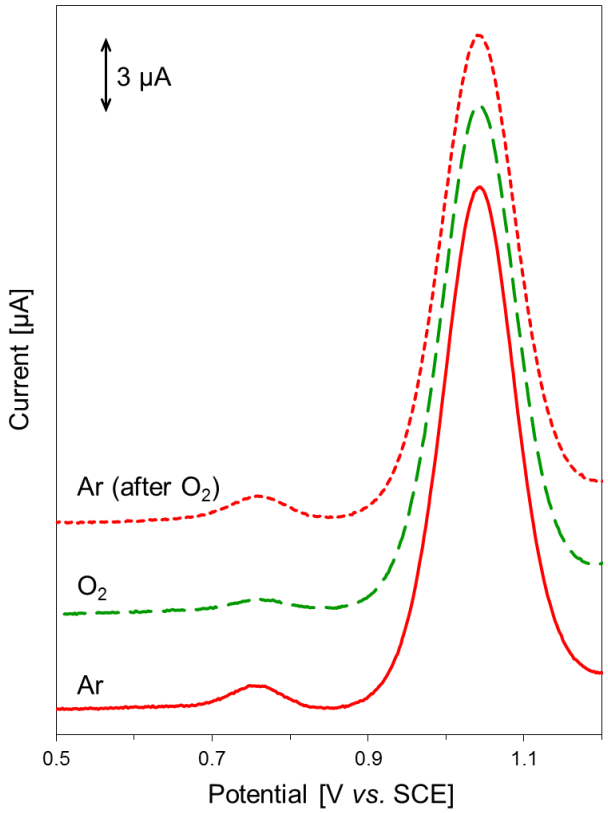

Figure 4 Thin layer square wave voltammograms of **$[Ru(bpy)_3](NO_3)_2 \cdot 5H_2O$** (1 mM) in a 0.1 M Na_2SO_4 aqueous solution with photoirradiation (400 nm < λ < 800 nm) under an Ar atmosphere (red) and an O_2 atmosphere (green). (WE: GC; CE: Pt wire; RE: SCE; scan rate: 5 mV s^{-1}).

3. Discussions

The results in Chapter 1 led us to investigate the photoelectrochemical properties of **Ru(bpy)$_3^{2+}$**, and electrochemical signals attributed to the photochemical reaction were successfully detected both by CV and SWV under thin layer conditions (Figs. 1-4).

Figure 5 shows a schematic diagram of the principle of excited state voltammetry. Photoexcited species is generated upon absorption of a photon. E_{ox}* and E_{red}* in Figure 5 indicate the oxidation and reduction potentials of the photoexcited species, respectively. When the potential of the working electrode (E) is between the first oxidation potential (E_{ox}) and first reduction potential (E_{red}) ($E_{red} < E < E_{ox}$), no redox reactions occur in the ground state. In the excited state, however, two opposite redox reactions, which are composed of the electron transfers from the photoexcited species to the electrode (oxidation) and from the electrode to the photoexcited species (reduction) occur at the same time. Therefore, the net current does not flow in this situation (a). When the electrode potential shifted more positive than E_{red}* ($E > E_{red}$*), the electron transfer from electrode to the photoexcited species corresponding to the oxidation of photoexcited species cannot occur, whereas the electron transfer from the photoexcited species to electrode can occur. Therefore, the anodic current flows and the resultant voltammogram gives the reduction potential of the excited state species, E_{red}* (b). By contrast, the oxidation potential of the excited state species, E_{ox}*, is determined from the cathodic voltammogram appeared at a more negative potential than E_{ox}* ($E < E_{ox}$*) (c). The above interpretation was previously explained in Ref. 7.

Based on the above interpretation, the peak at +0.8 V observed by SWV of **Ru(bpy)$_3^{2+}$** under photoirradiation is considered the reduction potential of the excited species (E_{red}*) of **Ru(bpy)$_3^{2+}$**, **[Ru(bpy)$_3$]$^{2+}$***. In addition, the E_{red}* value determined from the thin-layer SWV measurements under photoirradiation was found to be similar to the indirectly estimated values [8].

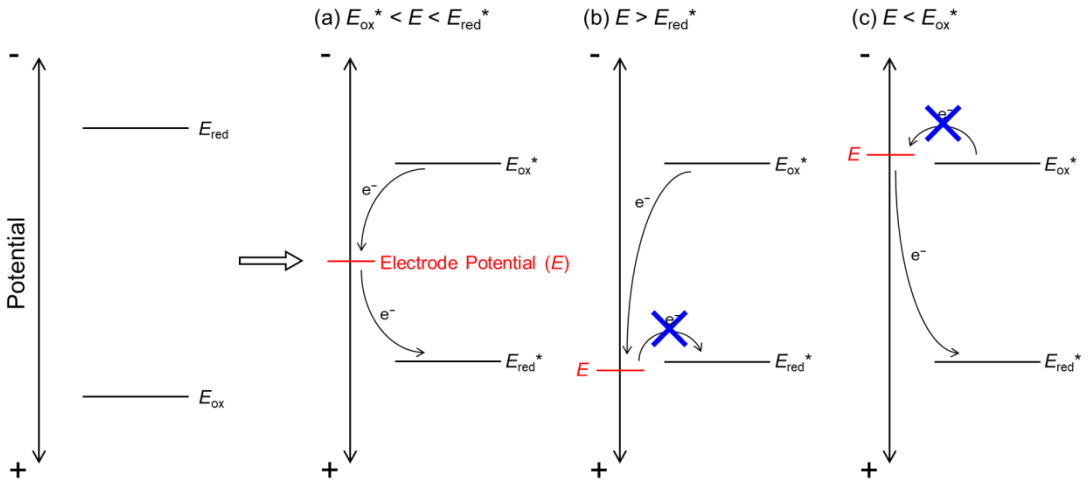

Figure 5 A schematic diagram of the principle of excited state voltammetry.

4. Conclusions

As a further extension of the study in Chapter 1, the thin layer voltammetry was performed to determine the redox potentials of a well-known metal-complex-based dye, tris(2,2'-bipyridyl)ruthenium(II) (**$[Ru(bpy)_3]^{2+}$**). In the voltammogram measured under photoirradiation, a broad peak appeared at approximately +0.8 V (*vs*. SCE), and the potential of the peak was similar to the reduction potential of **$[Ru(bpy)_3]^{2+}$*** calculated from the Rehm-Weller equation and the potential determined by electrochemical measurements. Moreover, the intensity of the peak drastically decreased under an O_2 atmosphere and was recovered by Ar bubbling. These results indicate that the peak originated from the triplet excited species of **$[Ru(bpy)_3]^{2+}$**, **$[Ru(bpy)_3]^{2+}$*** because this species is known to be quenched by triplet dioxygen. Although only the reduction potential of the **$[Ru(bpy)_3]^{2+}$*** was investigated in this work, this system has the possibility to apply for the detection of various photoexcited species.

5. Experimental Section

5.1. Materials

Na_2SO_4 was purchased from Wako Pure Chemical Industries, Ltd. **$[Ru(bpy)_3](NO_3)_2 \cdot 5H_2O$** was prepared as previously described [13]. All solvents and reagents were of the highest quality available and were used as received. H_2O was purified using a Millipore MilliQ purifier.

5.2. Measurements

All electrochemical measurements were conducted under argon. A three-electrode configuration was employed in conjunction with a Biologic SP-50 potentiostat interfaced to a computer with Biologic EC-Lab software. The measurements were performed using the system shown in Figure 1 in Chapter 1. The photoirradiation was performed using an ILC Technology CERMAX LX-300 Xe lamp (operated at 150 W unless otherwise mentioned) equipped with a CM-1 cold mirror (400 nm < λ < 800 nm). In some experiments, an OG570 longpass filter (λ > 570 nm, from SCHOTT) was used to select a specific wavelength region for photoirradiation. In all cases, a platinum wire counter electrode (diameter 0.5 mm, from BAS) and a GC disk working electrode (diameter 3 mm, from BAS) were used. The working electrode was treated between scans by means of polishing with 0.05 μm alumina paste (from BAS) and washing with purified H_2O. For all measurements, a saturated calomel electrode (SCE) was used for the reference electrode. The supporting electrolyte was 0.1 M Na_2SO_4. UV-visible absorption spectra were recorded on a SHIMADZU UV-1800 UV/Visible spectrophotometer.

References

1. H. Dau, I. Zaharieva, Principles, efficiency, and blueprint character of solar-energy conversion in photosynthetic water oxidation, Acc. Chem. Res. 42 (2009) 1861–1870.

2. K. Brettel, W. Leibl, Electron transfer in photosystem I, Biochim. Biophys. Acta 1507 (2001) 100–114.

3. D. G. Nocera, The artificial leaf, Acc. Chem. Res. 45 (2012) 767–776.

4. A. Magnuson, et. al. Biomimetic and microbial approaches to solar fuel generation, Acc. Chem. Res. 42 (2009) 1899–1909.

5. M. Grätzel, Conversion of sunlight to electric power by nanocrystalline dye-sensitized solar cells, J. Photochem. Photobiol. A: Chem. 164 (2004) 3–14.

6. W. E. Jones Jr., M. A. Fox, Determination of excited-state redox potentials by phase-modulated voltammetry, J. Phys. Chem. 98 (1994) 5095–5099.

7. N. Oda, K. Tsuji, A. Ichimura, Voltammetric measurements of redox potentials of photo-excited species, Anal. Sci. 17 (2001) i375–i378.

8. A. Juris. V. Balzani, F. Barigelletti, S. Campagna, P. Belser, A. V. Zelewsky, Ru(II) polypyridine complexes: photophysics, photochemistry, eletrochemistry, and chemiluminescence, Coord. Chem. Rev. 84 (1988) 85–277.

9. C. R. Bock, J. A. Connor, A. R. Gutierrez, T. J. Meyer, D. G. Whitten, B. P. Sullivan, J. K. Nagle, Estimation of excited-state redox potentials by electron-transfer quenching. Application of electron-transfer theory to excited-state redox processes, J. Am. Chem. Soc. 101 (1979) 4815–4824.

10. R. Ballardini, G. Varani, M. T. Indelli, F. Scandola, V. Balzani, Free energy correlation of rate constants for electron transfer quenching of excited transition metal complexes, J. Am. Chem. Soc. 100 (1978) 7219–7223.

11. J. Van Houten, R. J. Watts, Temperature dependence of the photophysical and photochemical properties of the tris(2,2'-bipyridyl)ruthenium(II) ion in aqueous solution, J. Am. Chem. Soc. 98 (1976) 4853–4858.

12. Quenching of triplet excited state of $Ru(bpy)_3^{2+}$ is known to proceed effectively by O_2. See the following reference, K. Kalyanasundaram, Photophysics, photochemistry and solar energy conversion with tris(bipyridyl)ruthenium(II) and its analogues, Coord. Chem. Rev. 46 (1982) 159–244.

13. R. A. Palmer, T. S. Piper, 2,2'-bipyridine complexes. I. polarized crystal spectra of tris(2,2'-bipyridine)copper(II), -nickel(II), -cobalt(II), -iron(II), and -ruthenium(II), Inorg. Chem. 5 (1966) 864–878.

Chapter 3

Analysis of photocatalytic reaction by *in-situ* cyclic voltammetry under photoirradiation

1. Introduction

Artificial photosynthesis, which is a representative example of solar-energy conversion systems, has attracted much attention due to its potential application in renewable energy [1]. To construct such artificial photosynthetic systems, the development of efficient catalysts for reactions involving multi-electron transfer, such as CO_2 reduction and water oxidation, is essential. There are two primary approaches to developing such catalysts: homogeneous [2] and heterogeneous systems [3]. Homogeneous catalysts such as metal complexes are advantageous for the analysis of their reaction mechanisms, including the respective photochemical and electrochemical processes, to allow for further modification of the catalyst design at the molecular level. To understand the detailed reaction mechanisms, the electrochemical response of the catalysts should be investigated under photoirradiation because the electrochemical process proceeds subsequent to the photochemical process in solar-energy conversion reactions. However, in general, the electrochemical and photochemical properties of molecular catalysts are separately evaluated using different experimental setups. To the best of our knowledge, there have been no reports on the electrochemical analysis of molecular catalytic systems in homogeneous solutions under photoirradiation.

Recently, we established a method to perform electrochemical analysis of photoirradiated solutions [4]. In our previous report, we measured cyclic voltammograms of ferrocene ($Fe(C_5H_5)_2$) under photoirradiation in a conventional electrochemical setup and obtained sigmoidal-shaped voltammograms that were unsuitable for the detailed analysis of the electrochemical processes. This result suggested that the photoirradiation may have generated convection due to local increases in temperature, and the mass transfer subsequently induced by this convection

affected the electrochemical responses. Based on this result, we aimed to decrease the unfavorable electrochemical response under photoirradiation and found three techniques (measurements with a rotating disk electrode (RDE), fast scanning, and thin layer cyclic voltammetry (TLCV)) that could suppress the aforementioned unfavorable current change. We also succeeded in detecting the electrochemical response of photochemically generated molecules using TLCV techniques.

As a further extension of our study, in this work, we applied our photo-electrochemical method for the analysis of catalytic systems. As a catalytic system, the CO_2 reduction reaction is an attractive target because molecules that can catalyze CO_2 reduction are longstanding targets for direct electrolytic fuel synthesis. Moreover, the capture and the efficient use of CO_2 is an important issue to resolve not only the shortage of fossil fuels but also global warming caused by increasing atmospheric CO_2 concentrations. In this contribution, the influence of photoirradiation on the electrochemical CO_2 reduction reaction catalyzed by *meso*-tetraphenylporphyrin iron(III) chloride (**Fe(tpp)Cl**) [5,6] was analyzed using the electrochemical technique.

2. Results and discussion

A cyclic voltammogram of **Fe(tpp)Cl** measured by the conventional technique is shown in Figure 1a. The voltammograms were measured in 0.1 M tetra(*n*-butyl)ammonium perchlorate (TBAP)/*N*,*N*-dimethylformamide (DMF). Under an Ar atmosphere in dark conditions, the voltammogram displayed three reversible reduction waves at $E_{1/2}$ (half-wave potentials) = −0.6, −1.5 and −2.1 V *vs.* ferrocenium/ferrocene (Fc^+/Fc), which were assigned as Fe(III)/Fe(II), Fe(II)/Fe(I) and Fe(I)/Fe(0) redox couples, respectively [6]. Under photoirradiation using a Xe lamp with a CM-1 cold mirror (400-800 nm), the shape of the voltammogram dramatically changed, and the current that was attributed to the convection induced by the photoirradiation was observed. These results indicated that the analysis of the photoelectrochemical response of **Fe(tpp)Cl** was not allowed with the conventional technique. By contrast, the measurements using the TLCV technique with a layer thickness (*d*, Figure 1c) of 0.25 mm gave different results. As shown in Figure 1b, under dark conditions, three reversible redox waves were observed at approximately the same potentials as those obtained in the conventional measurement. Under photoirradiation, the same three reversible reduction waves were observed, maintaining the shape of the voltammogram. Therefore, the convection induced by photoirradiation was suggested to be suppressed in the TLCV measurements, and it was confirmed that the electrochemical measurement of **Fe(tpp)Cl** under photoirradiation could be performed using the TLCV technique.

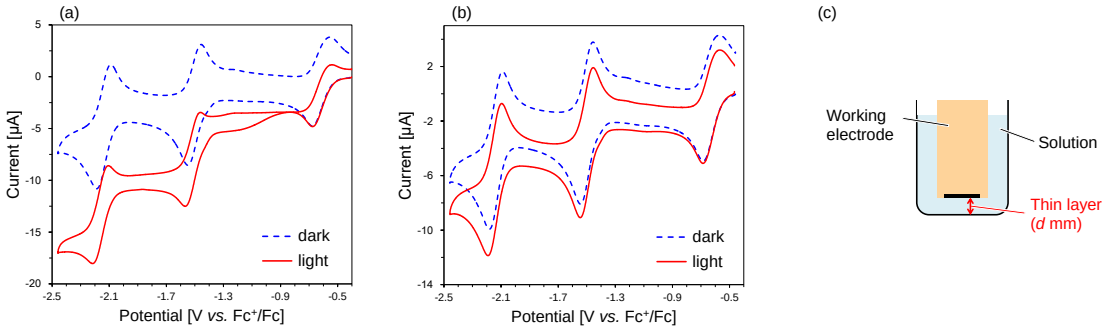

Figure 1 (a) Cyclic voltammograms (d = 5 mm) with Fe(III)/Fe(II), Fe(II)/Fe(I) and Fe(I)/Fe(0) redox waves. (b) Thin layer cyclic voltammograms (d = 0.25 mm) with Fe(III)/Fe(II), Fe(II)/Fe(I) and Fe(I)/Fe(0) redox waves. (c) Schematic illustration of the thickness of the solution layer. CV measurements were performed with **Fe(tpp)Cl** (1 mM) in a 0.1 M TBAP / DMF solution with photoirradiation (red, 400 nm < λ < 800 nm) and without photoirradiation (blue) under an Ar atmosphere (WE: GC; CE: Pt wire; RE: Ag^{+}/Ag; scan rate: 20 mV s^{-1}).

TLCV measurements of **Fe(tpp)Cl** were also performed under a CO_2 atmosphere to analyze the catalytic reduction of CO_2. In the voltammogram of **Fe(tpp)Cl** under dark conditions (Figure 2), the first and second reduction peaks were observed at the exact same potentials as those observed under Ar conditions. Additionally, large irreversible cathodic currents were observed at the potential corresponding to the Fe(I)/Fe(0) redox couple (−2.1 V *vs.* Fc^+/Fc), indicating the electrocatalytic CO_2 reduction to CO. In the subsequent anodic scan in the positive direction, the irreversible wave was observed at approximately E_{pa} = −1.7 V *vs.* Fc^+/Fc, and the original re-oxidation waves observed at E_{pa} = −0.6 and −1.5 V under an Ar atmosphere were not detected (Figure 2, blue line). By contrast, under photoirradiation, the two reversible redox waves at $E_{1/2}$ = −0.6 and −1.5 V and the catalytic currents at approximately −2.1 V were observed (Figure 2, red line). It should be noted that the intensity of the irreversible wave at E_{pa} = −1.7 V, which was observed in the measurements under dark conditions, dramatically decreased in the voltammogram under photoirradiation. These results clearly indicated that photoirradiation largely affected the redox properties of **Fe(tpp)Cl** under a CO_2 atmosphere.

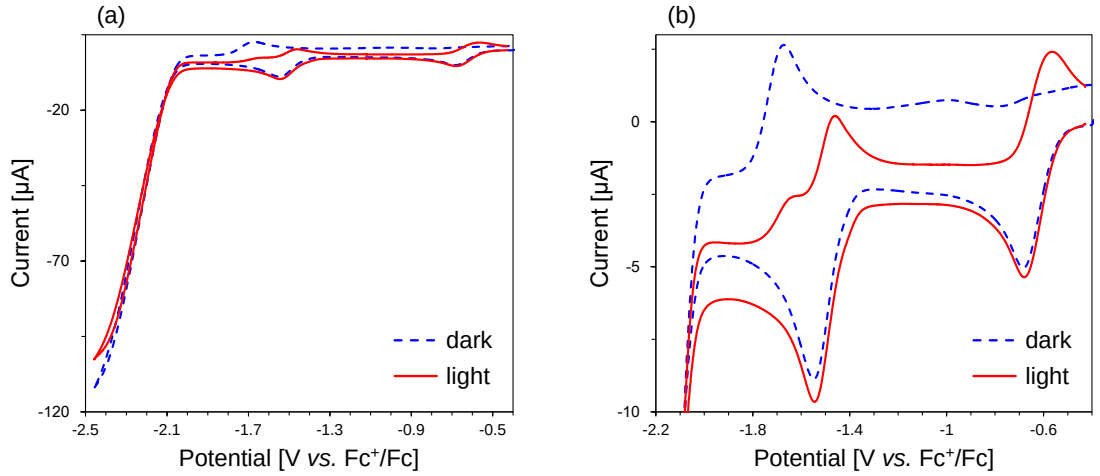

Figure 2 Thin layer cyclic voltammograms (d = 0.25 mm) of **Fe(tpp)Cl** (1 mM) in a 0.1 M TBAP / DMF solution with photoirradiation (red, 400 nm < λ < 800 nm) and without photoirradiation (blue) under a CO_2 atmosphere (WE: GC; CE: Pt wire; RE: Ag^+/Ag; scan rate: 20 mV s^{-1}). (a) Voltammograms with a catalytic current. (b) Enlarged voltammograms focusing on Fe(III)/Fe(II) and Fe(II)/Fe(I) redox waves.

To further understand this phenomenon, several electrochemical measurements were performed in thin-layer conditions under a CO_2 atmosphere. First, chronoamperometry was performed both under photoirradiation and in the dark. The solution of **Fe(tpp)Cl** (1 mM) in DMF containing TBAP (0.1 M) was electrolyzed at the GC electrode with a cell operating potential of −2.3 V *vs.* Fc^+/Fc while keeping the layer thickness as 0.25 mm. As shown in Figure 3, constant currents flowed during the 300 seconds of electrolysis, and the intensities of the currents were almost the same irrespective of the photoirradiation. From these results, it was assumed that the catalytic current of CO_2 reduction catalyzed by **Fe(tpp)Cl** was not affected by photoirradiation.

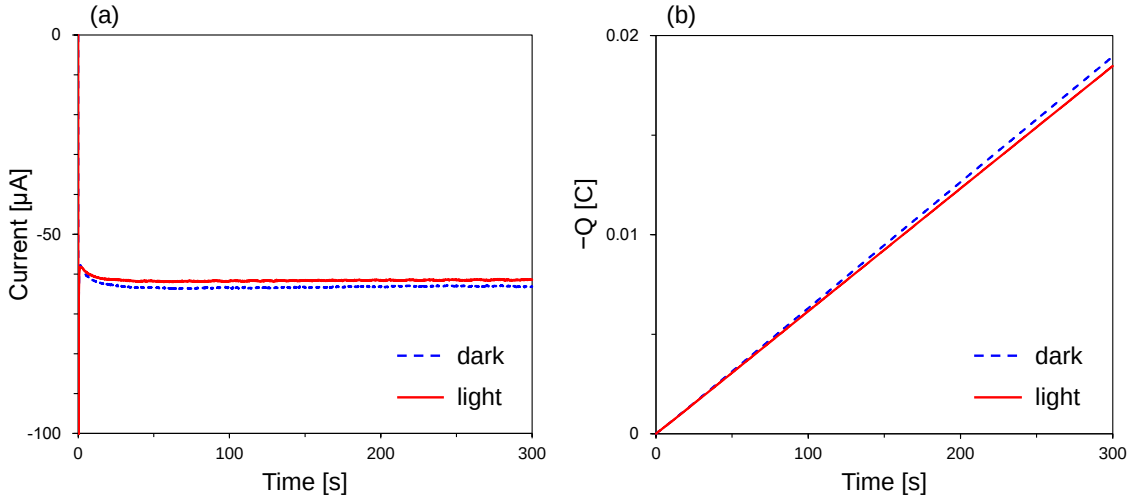

Figure 3 Thin layer chronoamperograms (E = −2.3 V *vs.* Fc^+/Fc, d = 0.25 mm) of **Fe(tpp)Cl** (1 mM) in a 0.1 M TBAP / DMF solution with photoirradiation (red, 400 nm < λ < 800 nm) and without photoirradiation (blue) under a CO_2 atmosphere (WE: GC; CE: Pt wire; RE: Ag^+/Ag). (a) Time *vs.* Current. (b) Time *vs.* Coulombs.

Second, the origin of the irreversible peak at approximately −1.7 V under the dark conditions was investigated by changing the negative edges of the potential sweep. Figure 4 shows the voltammograms of **Fe(tpp)Cl** for which the negative edges of the potential sweep were −2.5 (blue line), −2.2 (green line) and −2.1 V (red line). Although the shapes of the voltammograms were almost the same when the measurements were performed under photoirradiation, a clear difference was observed in the measurement under the dark condition. For the negative edge located at −2.1 V, which was more positive than the CO_2 reduction potential catalyzed by **Fe(tpp)Cl**, the second redox wave was reversibly observed. By shifting the negative edges to the negative region, the irreversible peak at −1.7 V gradually appeared, and the intensity of the peak at E_{pa} = −1.5 V decreased. These observations suggested that the flow of the large catalytic current induced the generation of the irreversible peak at −1.7 V.

Finally, the dependence of the generation of the irreversible peak on the light intensity was investigated. Figure 5 shows the cyclic voltammogram of **Fe(tpp)Cl** under photoirradiation with different intensities of light (150 and 300 W). When the light intensity was increased, the peak height of the irreversible wave at −1.7 V decreased, and the original re-oxidation wave at E_{pa} = −1.5 V increased. From these results, the generation of the irreversible peak around −1.7 V was presumed to be effectively suppressed by photoirradiation.

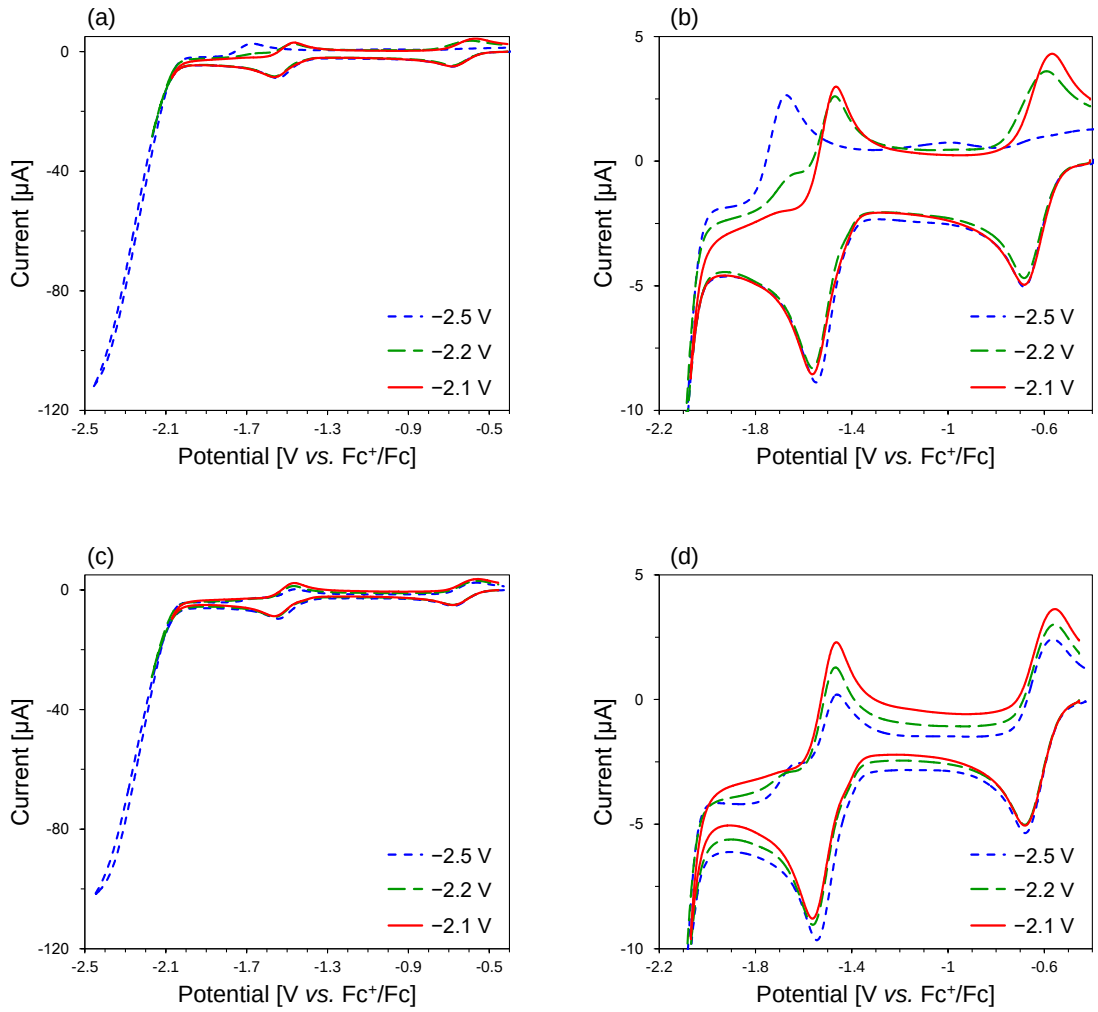

Figure 4 Thin layer cyclic voltammograms (d = 0.25 mm) of **Fe(tpp)Cl** (1 mM) in a 0.1 M TBAP / DMF solution for which the negative edges of the potential sweep were −2.5 V (blue), −2.2 V (green) and −2.1 V (red) (WE: GC; CE: Pt wire; RE: Ag^{+}/Ag; scan rate: 20 mV s^{-1}). (a) Voltammograms showing the negative edges of potential sweeping without photoirradiation. (b) Enlarged voltammograms focusing on Fe(III)/Fe(II) and Fe(II)/Fe(I) redox waves without photoirradiation. (c) Voltammograms showing the negative edges of potential sweeping with photoirradiation. (d) Enlarged voltammograms focusing on Fe(III)/Fe(II) and Fe(II)/Fe(I) redox waves with photoirradiation.

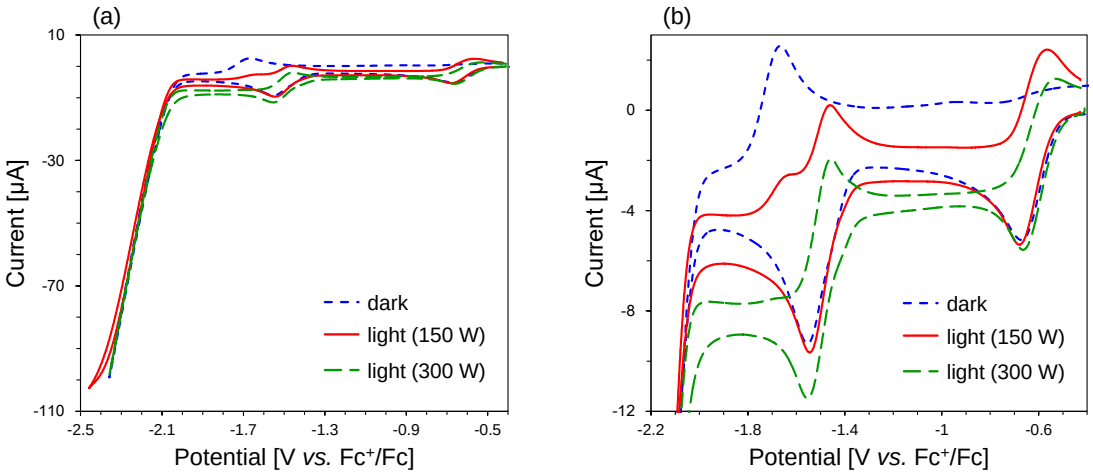

Figure 5 Thin layer cyclic voltammograms (d = 0.25 mm) of **Fe(tpp)Cl** (1 mM) in a 0.1 M TBAP / DMF solution with photoirradiation in various light intensities (red, 150 W; green, 300 W) and without photoirradiation (blue) under a CO_2 atmosphere (WE: GC; CE: Pt wire; RE: Ag^+/Ag, scan rate: 20 mV s^{-1}). (a) Voltammograms showing a catalytic current. (b) Enlarged voltammograms focusing on Fe(III)/Fe(II) and Fe(II)/Fe(I) redox waves.

The aforementioned observations enabled us to describe the effect of photoirradiation on the redox properties of **Fe(tpp)Cl** in combination with the proposed catalytic cycle. The proposed reaction mechanism of electrocatalytic CO_2 reduction by **Fe(tpp)Cl** was reported by Savéant *et al.* [6] and is summarized in Scheme 1. Initially, **Fe(tpp)Cl** is reduced from Fe(III) to Fe(0) by the sequential one-electron reduction processes; these processes were observed in the measurement under an Ar atmosphere (*vide supra*). The generated Fe(0) species react with CO_2, and the CO_2-bound complexes forms. Subsequent adduction of acid (in this case, the hydrated water of the catalyst) and the C-O bond cleavage reaction in coordination with proton transfer result in the formation of the CO-bound complex. Further reaction with the Fe(0) species leads to the generation of CO. It was also reported that CO generated by the catalytic reaction could bind to catalysts with the Fe(I) state as the side reaction of the CO_2 reduction reaction by **Fe(tpp)Cl** (I in Scheme 1), and the electrochemical response corresponding to this side reaction was observed at approximately −1.7 V. Similarly, the irreversible peak, which was attributed to the side reaction, was detected at −1.7 V in

our experiments using the TLCV technique in the dark condition. Furthermore, we found that the intensity of the peak decreased upon photoirradiation and, in some conditions, the electrochemical response of the side reaction could be suppressed. A reasonable explanation of this phenomenon is given by considering the photoinduced decarbonylation from carbonyliron tetraphenylporphyrin [7]. As shown in Figure 2b, the irreversible peak assigned to the oxidative Fe-CO reassociation ($[Fe^{I}(tpp)]^{-}$ + CO → $[Fe^{II}(tpp)CO]$ + e^{-}, I in Scheme 1) was observed at $E_{pa} \approx -1.7$ V in the positive-direction sweeping in the dark condition. Under photoirradiated condition, the photoinduced decarbonylation reaction of $[Fe^{II}(tpp)CO]$ proceeds to afford $[Fe^{II}(tpp)]$ ($[Fe^{II}(tpp)CO]$ + $h\nu \rightarrow [Fe^{II}(tpp)]$ + CO) [7]. The photochemically generated $[Fe^{II}(tpp)]$ is successively reduced ($[Fe^{II}(tpp)]$ + $e^{-} \rightarrow [Fe^{I}(tpp)]^{-}$, $E_{1/2} \approx -1.5$ V, II in Scheme 1). As a result, the current attributed to the oxidative Fe-CO reassociation (I in Scheme 1) is offset by the current attributed to the reduction of the photochemically generated $[Fe^{II}(tpp)]$ (II in Scheme 1). In total, the electrochemical response of the side reaction in the catalytic system could be hindered by photoirradiation.

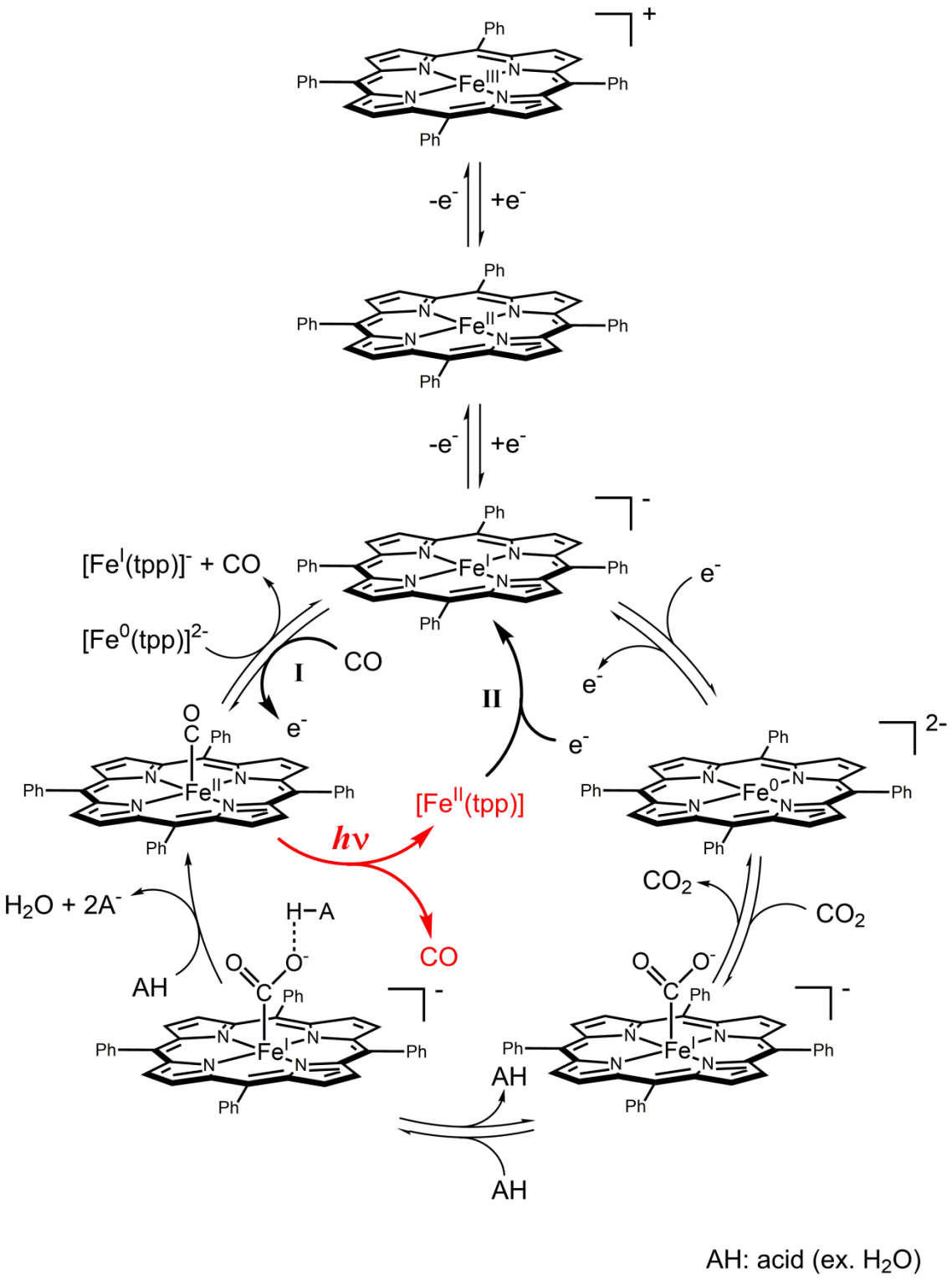

Scheme 1. Proposed mechanism of the catalytic reaction [6]. The coordination of solvent molecules and counter anions is in equilibrium [8] and omitted for clarity.

3. Conclusions

In conclusion, the author first demonstrated the electrochemical analysis of a catalytic system under photoirradiation. A well-known catalyst for CO_2 reduction, **Fe(tpp)Cl**, was selected as a target analyte, and the electrochemical response of the catalyst was successfully investigated using the TLCV technique. Under a CO_2 atmosphere, the catalytic current originating from CO_2 reduction was observed both under the dark and light conditions. Under the dark conditions, an irreversible re-oxidation wave was observed at −1.7 V *vs.* Fc^+/Fc in the voltammogram. Under photoirradiation, on the other hand, the intensity of the irreversible peak dramatically decreased; however, the intensities of the reversible peaks originating from the redox of the catalyst increased. Further electrochemical measurements with various conditions revealed that the generation of the irreversible peak depended on the negative edges of the potential sweep and the intensity of the light used in photoirradiation. Moreover, it was found that the original [Fe^{II}(tpp)] complex is regenerated by the photoinduced CO dissociation from [Fe^{II}(tpp)CO] based on the analysis of these electrochemical responses in combination with the proposed reaction mechanism. These results show that the method presented in this contribution has the possibility of analyzing various catalytic reactions.

4. Experimental Section

4.1. Materials

Pyrrole was purchased from Sigma-Aldrich Co., LLC. Benzaldehyde, propanoic acid, hydrochloric acid and ferrocene (**Fc**) were purchased from Wako Pure Chemical Industries, Ltd. $FeCl_2 \cdot 4H_2O$ and *N*,*N*-dimethylformamide (DMF) were purchased from Kanto Chemical Co., Inc. Tetra(*n*-butyl)ammonium perchlorate (TBAP) was purchased from Tokyo Chemical Industry Co., Ltd. All of the solvents and reagents were of the highest quality available and were used as received, except for TBAP and DMF for the electrochemical measurements. TBAP was recrystallized from absolute ethanol and dried in vacuo. DMF was degassed and purified under N_2 atmosphere using a GlassContour solvent system (Nikko Hansen Co., Ltd.).

4.2. Syntheses

*4.2.1. Synthesis of meso-tetraphenylporphyrin (**H_2(tpp)**)*

H_2(tpp) was prepared as previously described [9]. Pyrrole (1.7 mL, 25 mmol) and benzaldehyde (2.6 mL, 25 mmol) were dissolved in propanoic acid (50 mL), then refluxed for 1 h and cooled to room temperature. The resulting mixture was filtered and washed with methanol. Recrystallization from CH_2Cl_2/methanol gave a purple solid. ^{1}H NMR ($CDCl_3$): δ-2.80 (s, 2H), 7.71-7.78 (m, 12H), 8.19-8.21 (m, 8H), 8.82 (s, 8H).

*4.2.2. Synthesis of meso-tetraphenylporphyrin iron(III) chloride (**Fe(tpp)Cl**)*

Fe(tpp)Cl was prepared by the modification of a previous report [10]. To a solution of **H_2(tpp)** (200 mg, 0.32 mmol) in *N*,*N*-dimethylformamide (DMF) (70 mL), a DMF (60 mL) solution of $FeCl_2 \cdot 4H_2O$ (388 mg, 1.95 mmol) was added dropwise at room temperature. The mixture was refluxed for 1 h and then cooled to room temperature. Diluted hydrochloric acid (HCl) (6 M, 80 mL) was added to the resulting solution. A purple solid was collected by filtration and washed with 3 M HCl. The compound was identified by elemental analysis. Found: C, 73.63; H, 4.21; N, 7.97. Calcd for $C_{44}H_{29.4}ClFeN_4O_{0.7}$ ([**Fe(tpp)Cl**]·$0.7H_2O$): C, 73.74; H, 4.14; N, 7.82.

4.3. Measurements

All of the electrochemical measurements were conducted under argon unless otherwise mentioned. A three-electrode configuration was employed in conjunction with a Biologic SP-50 potentiostat that interfaced with a computer with Biologic EC-Lab software. The measurements were performed using the system shown in Figure 1 in Chapter 1 to avoid photoirradiation of the reference electrode and the counter electrode. The photoirradiation was performed using an ILC Technology CERMAX LX-300 Xe lamp (operated at 150 W unless otherwise mentioned) equipped with a CM-1 cold mirror (400 nm < λ < 800 nm). In all cases, a platinum wire counter electrode (diameter 0.5 mm, from BAS) and a glassy carbon (GC) disk working electrode (diameter 3 mm, from BAS) were used. The working electrode was treated between scans by means of polishing with 0.05-μm alumina paste (from BAS) and washing with purified H_2O. For all measurements, an Ag^+/Ag reference electrode was used. The supporting electrolyte was 0.1 M TBAP. The potentials reported within these measurements were referenced to the Fc^+/Fc couple at 0 V.

References

1. (a) D. G. Nocera, The artificial leaf, Acc. Chem. Res. 45 (2012) 767–776. (b) D. Gust, T. A. Moore, A. L. Moore, Solar fuels via artificial photosynthesis, Acc. Chem. Res. 42 (2009) 1890–1898.

2. (a) C. W. Cady, R. H. Crabtree, G. W. Brudvig, Functional models for the oxygen-evolving complex of photosystem II, Coord. Chem. Rev. 252 (2008) 444–455. (b) H. Takeda, O. Ishitani, Development of efficient photocatalytic systems for CO_2 reduction using mononuclear and multinuclear metal complexes based on mechanistic studies, Coord. Chem. Rev. 254 (2010) 346–354.

3. (a) A. Kudo, Y. Miseki, Heterogeneous photocatalyst materials for water splitting, Chem. Soc. Rev. 38 (2009) 253–278. (b) K. Maeda, K. Domen, Photocatalytic water splitting: recent progress and future challenges, J. Phys. Chem. Lett. 1 (2010) 2655–2661. (c) R. Abe, Recent progress on photocatalytic and photoelectrochemical water splitting under visible light irradiation, J. Photochem. Photobiol. C: Photochem. Rev. 11 (2010) 179–209.

4. A. Fukatsu, M. Kondo, M. Okamura, M. Yoshida, S. Masaoka, Electrochemical response of metal complexes in homogeneous solution under photoirradiation, Sci. Rep. 4 (2014) 5327.

5. I. Bhugun, D. Lexa, J.-M. Savéant, Ultraefficient selective homogeneous catalysis of the electrochemical reduction of carbon dioxide by an iron(0) porphyrin associated with a weak Brönsted acid cocatalyst, J. Am. Chem. Soc. 116 (1994) 5015–5016.

6. C. Costentin, S. Drouet, G. Passard, M. Robert, J.-M. Savéant, Proton-coupled electron transfer cleavage of heavy-atom bonds in electrocatalytic processes. Cleavage of a C−O bond in the catalyzed electrochemical reduction of CO_2, J. Am. Chem. Soc. 135 (2013) 9023–9031.

7. M. Hoshino, K. Ueda, M. Takahashi, M. Yamaji, Y. Hama, Y. Miyazaki, Photoinduced decarbonylation from carbonyliron tetraphenylporphyrin in ethanol. Effects of axial imidazole studied by laser flash photolysis, J. Phys. Chem. 96 (1992) 8863–8870.

8. K. M. Kadish, E. V. Caemelbecke, G. Royal, Electrochemistry of metalloporphyrins in nonaqueous media, in: K. M. Kadish, K. M. Smith, R. Guilard (Eds.), The Porphyrin Handbook, vol. 8, Academic Press, San Diego, 2000, pp. 1–114.

9. A. D. Adler, F. R. Longo, W. Shergalis, Mechanistic investigations of porphyrin syntheses. I. preliminary studies on *ms*-tetraphenylporphin, J. Am. Chem. Soc. 86 (1964) 3145–3149.

10. H. Kobayashi, T. Higuchi, Y. Kaizu, H. Osada, M. Aoki, Electronic spectra of tetraphenylporphinatoiron (III) methoxide, Bull. Chem. Soc. Jpn. 48 (1975) 3137–3141.

Acknowledgements

The presented thesis is the summary of my studies from April 2013 to March 2018 at the Department of Structural Molecular Science, School of Physical Science, SOKENDAI (the Graduate University for Advanced Studies) under the direction of Dr. Shigeyuki Masaoka, Associate Professor of SOKENDAI.

I would like to express my deepest gratitude to my supervisor, Associate Professor Dr. Shigeyuki Masaoka for his significant guidance, impassioned encouragement and valuable discussion. I could learn much from him not only chemistry but also the passion toward science. I would like to express my sincere appreciation to Assistant Professor Dr. Mio Kondo for her heartfelt encouragement, incomparable kindness, and instructive direction. I would like to express my sincere thanks to Designated Assistant Professor Dr. Masaya Okamura in Nagoya University for many beneficial advices about research and valuable discussion.

I would like to express my sincere appreciation to Professor Dr. Hiroshi Yamamoto, Professor Dr. Toshihiko Yokoyama, Associate Professor Dr. Yuji Furutani in Institute for Molecular Science, and Associate Professor Dr. Katsuhiko Kanaizuka in Yamagata University for being my thesis examiner and giving the valuable suggestions and corrections to my work, which greatly helped me to improve in various aspects.

I would like to express my gratitude to Assistant Professor Dr. Masaki Yoshida in Hokkaido University for many advices about research, valuable discussion and heartfelt encouragement.

I am deeply grateful to Mr. Nobuo Mizutani and Mr. Takayuki Yano in Institute for Molecular Science for manufacture of the photoelectrochemical cell. I am also deeply grateful to Mr. Tadakazu Omaru in Institute for Molecular Science for making the glass cell.

I am deeply grateful to Mr. Seiji Makita in Institute for Molecular Science for the measurement of elemental analysis. I am also deeply grateful to Ms. Michiko Nakano and Ms. Haruyo Nagao in Institute for Molecular Science for the measurement of ^{1}H-NMR spectroscopy.

I am deeply grateful to Ms. Sena Torii and Ms. Akane Shibata in Institute for Molecular Science for the preparation of **[Ru(bpy)$_3$](NO$_3$)$_2$**. I am also deeply grateful to Dr. Yuki Okabe in Institute for Molecular Science for the preparation of **Fe(tpp)Cl**.

I would like to express my sincere appreciation to our members in Institute for Molecular Science, Dr. Praneeth Vijayendran, Ms. Pondchanok Chinapang, Mr. Sze Koon Lee, Mr. Hitoshi Izu, Mr. Takafumi Enomoto, Mr. Riku Ushijima, Ms. Chihiro Matsui, Ms. Mami Kachi, Ms. Masahiro Tasaki, Ms. Mari Kanaike, Ms. Akane Shibata and Ms. Miho Matsuda for many advices about research, valuable discussion, heartfelt encouragement and friendship during my time in the lab. I also wish to express my sincere thanks to our former members, Dr. Go Nakamura, Dr. Takahiro Itoh, Dr. Yuki Okabe, Mr. Ke Liu, Ms. Yukino Fukahori, Ms. Reiko Kuga and Ms. Kaori Wakabayashi. I am also deeply grateful to Ms. Mayuko Taniwake and Ms. Kyoko Nogawa, for their warmhearted encouragement and technical support.

I would like to express my sincere appreciation to Professor Dr. Marc Robert, Senior Scientist Dr. Benoît Limoges, Associate Professor Dr. François Mavré, Dr. Iban Azcarate and all members in Laboratoire d'Electrochimie Moléculaire, Université Paris Diderot for many helpful advices and invaluable experiences through the internship.

I would like to express my sincere thanks to Professor Dr. Hiroshi Yamamoto, Ms. Noriko Takada and Ms. Michiko Nakano in Institute for Molecular Science, Professor Dr. Tomonori Usuda, Assistant Professor Dr. Norio Narita and his group members in National Astronomical Observatory of Japan for their significant guidance, helpful suggestion and valuable discussion during the lab rotation.

I would like to express my gratitude to Professor Dr. Hiroshi Yamamoto, Associate Professor Dr. Yuji Furutani and Associate Professor Dr. Nobuyasu Koga in Institute for Molecular Science, Assistant Professor Dr. Ryutaro Tokutsu in National Institute for Basic Biology, and Associate Professor Dr. Ryugo Tero in Toyohashi University of Technology for valuable discussion and invaluable experiences through the NINS Program for Cross-Disciplinary Study.

I also gratefully acknowledges Professor Dr. Hidehiro Sakurai in Osaka University, Associate Professor Dr. Shuhei Higashibayashi in Keio University, Associate Professor Dr. Norie Momiyama, Assistant Professor Dr. Atsuto Izumiseki, Assistant Professor Dr. Takuya, Kurahashi in the Institute for Molecular Science, Assistant Professor Dr. Koji Yamamoto in Tokyo Institute of Technology, and the other members in the Yamate Joint Seminar for valuable comments to my work and fruitful discussion of chemistry.

I would like to thank everyone who gave me valuable advice and precise comments to my work.

I am gratefully acknowledges the financial support of the Research Fellowships of the Japan Society for the Promotion of Science for Young Scientists, IMS Scholarship of Institute for Molecular Science and Course-by-Course Education Program to Cultivate Researchers in Physical Sciences with Broad Perspectives of SOKENDAI.

Finally, I offer thanks to my family, for their continuous, warmhearted encouragement and financial support.

Arisa Fukatsu

March, 2018

List of publications

Chapter 1 & 2

"Electrochemical response of metal complexes in homogeneous solution under photoirradiation"

Arisa Fukatsu, Mio Kondo, Masaya Okamura, Masaki Yoshida and Shigeyuki Masaoka

Scientific Reports, **2014**, *4*, 5327.

Chapter 3

"Electrochemical analysis of iron-porphyrin-catalyzed CO_2 reduction under photoirradiation"

Arisa Fukatsu, Mio Kondo, Yuki Okabe and Shigeyuki Masaoka

Journal of Photochemistry and Photobiology A: Chemistry, **2015**, *313*, 143–148.

(Themed Issue: Artificial Photosynthesis)

Another publication

"Hybrid Catalysis Enabling Room-Temperature Hydrogen Gas Release from *N*-Heterocycles and Tetrahydronaphthalenes"

Shota Kato, Yutaka Saga, Masahiro Kojima, Hiromu Fuse, Shigeki Matsunaga, **Arisa Fukatsu**, Mio Kondo, Shigeyuki Masaoka and Motomu Kanai

Journal of the American Chemical Society, **2017**, *139*, 2204–2207.